High resolution crystal structures of the Escherichia coli lytic transglycosylase Slt70 and its complex with a peptidoglycan fragment

Asselt, Erik J. van; Thunnissen, Andy-Mark W.H.; Dijkstra, Bauke W.

Published in:
Journal of Molecular Biology

DOI:
10.1006/jmbi.1999.3013

Article No. jmbi.1999.3013 available online at http://www.idealibrary.com on IDEAL® J. Mol. Biol. (1999) 291, 877–898

JMB

High Resolution Crystal Structures of the *Escherichia coli* Lytic Transglycosylase Slt70 and its Complex with a Peptidoglycan Fragment

Erik J. van Asselt, Andy-Mark W. H. Thunnissen and Bauke W. Dijkstra*

BIOSON Research Institute Laboratory of Biophysical Chemistry, University of Groningen, Nijenborgh 4 9747 AG Groningen, The Netherlands

*Corresponding author

The 70 kDa soluble lytic transglycosylase (Slt70) from *Escherichia coli* is an exo-muramidase, that catalyses the cleavage of the glycosidic bonds between *N*-acetylmuramic acid and *N*-acetylglucosamine residues in peptidoglycan, the main structural component of the bacterial cell wall. This cleavage is accompanied by the formation of a 1,6-anhydro bond between the C1 and O6 atoms in the *N*-acetylmuramic acid residue (anhMurNAc). Crystallographic studies at medium resolution revealed that Slt70 is a multi-domain protein consisting of a large ring-shaped α-superhelix with on top a catalytic domain, which resembles the fold of goose-type lysozyme. Here we report the crystal structures of native Slt70 and of its complex with a 1,6-anhydromuropeptide solved at nominal resolutions of 1.65 Å and 1.90 Å, respectively. The high resolution native structure reveals the details on the hydrogen bonds, electrostatic and hydrophobic interactions that stabilise the catalytic domain and the α-superhelix. The building-block of the α-superhelix is an ''up-down-up-down'' four-α-helix bundle involving both parallel and antiparallel helix pairs. Stabilisation of the fold is provided through an extensive packing of apolar atoms, mostly from leucine and alanine residues. It lacks, however, an internal consensus sequence that characterises other super-secondary helical folds like the β-helix in pectate lyase or the (β-α)-helix in the ribonuclease inhibitor. The 1,6-anhydromuropeptide product binds in a shallow groove adjacent to the peptidoglycan-binding groove of the catalytic domain. The groove is formed by conserved residues at the interface of the catalytic domain and the α-superhelix. The structure of the Slt70-1,6-anhydromuropeptide complex confirms the presence of a specific binding-site for the peptide moieties of the peptidoglycan and it substantiates the notion that Slt70 starts the cleavage reaction at the anhMurNAc end of the peptidoglycan.

Keywords: lytic transglycosylase; peptidoglycan; crystal structure; α-superhelix; 1,6-anhydromuropeptide

Introduction

Structural integrity of the bacterial cell wall is of vital importance for the prokaryotic cell. Without a rigid, intact cell wall, bacteria are not able to maintain their specific shapes. They may become spherical and burst as they are no longer able to resist the osmotic pressure inside their cells. The stress-resistant cell wall is, however, not a static structure: It has to increase in size to allow cell growth. Moreover, it is intimately involved in cell division, which requires precisely localised synthesis and cleavage of cell wall material (Schwarz *et al.*, 1969;

Abbreviations used: Slt70, 70 kDa soluble lytic transglycosylase; T4L, T4 phage lysozyme; GlcNAc, *N*-acetylglucosamine; MurNAc, *N*-acetylmuramic acid; anhMurNAc, 1,6-anhydro-*N*-acetylmuramic acid; G(anh)MTri, *N*-acetylglucosamyl-1,6-anhydro-*N*-acetylmuramyl-L-alanyl-D-glutamyl-*meso*-diaminopimelic acid (GlcNAc-anhMurNAc-L-Ala-D-Glu-*m*-Dap).

E-mail address of the corresponding author: bauke@chem.rug.nl

0022-2836/99/340877–22 $30.00/0

Romeis *et al*., 1991). The simultaneous requirements for both rigidity and flexibility of the bacterial cell wall have been combined in a unique molecular meshwork known as murein or peptidoglycan. This is a biopolymer built up of linear glycan strands, that are cross-linked by short peptides, thus forming a network-like structure that surrounds the cytoplasmic membrane of the bacterial cell as one giant macromolecule (Weidel & Pelzer, 1964). Growth and division of the cell wall polymer are believed to result from a balanced action of murein-synthesising and murein-degrading enzymes (Höltje & Schwarz, 1985). In this finely tuned interplay of metabolic enzymes, the murein-degrading enzymes are considered to fulfil a number of fundamental tasks (Shockman & Höltje, 1994; Höltje, 1998). Apart from taking care of specific cleavage of murein during cell division, they serve as ''space makers'' during cell growth, providing space and acceptor sites for incoming new murein material. In addition they form part of the peptidoglycan turnover and recycling system enabling the cell to make efficient use of old murein material for remodelling and enlargement of the cell wall. Unfortunately, knowledge of the precise biological functions of these enzymes, and of the mechanism by which the bacterium controls their lytic activity is still lacking.

Among the murein-degrading enzymes in the Gram-negative bacterium *Escherichia coli*, the lytic transglycosylases are of special interest. By cleaving the β-1,4-glycosidic bonds between the *N*-acetylmuramic acid (MurNAc) and *N*-acetylglucosamine (GlcNAc) residues of the glycan strands, these bacterial muramidases are able to totally degrade intact murein *in vitro*, as do various lysozymes. However, completely unlike lysozymes, they catalyse, concomitantly to cleavage, the synthesis of a new intramolecular glycosidic bond between carbons 1 and 6 of the MurNAc residue thereby forming a non-reducing 1,6-anhydro-*N*-acetylmuramic acid (anhMurNAc, Figure 1) (Höltje *et al*., 1975). Six different lytic transglycosylases have been isolated from *E. coli*. One is a soluble enzyme located in the periplasmic space with molecular mass of 70 kDa (Slt70) (Engel *et al*., 1991), the other five enzymes are membrane-bound lipo-proteins (MltA-D, EmtA) (Engel *et al*., 1992; Ursinus & Höltje, 1994; Dijkstra *et al*., 1995; Ehlert *et al*., 1995; Dijkstra, 1997; Lommatzsch *et al*., 1997; Kraft *et al*., 1998). They differ in their substrate preferences, in their enzymatic activity and in their susceptibilities towards certain glycopeptide inhibitors (Romeis *et al*., 1993). Slt70 has been characterised in most detail. The gene of Slt70 has been cloned and sequenced (Betzner & Keck, 1989; Engel *et al*., 1991) and it encodes a monomeric enzyme of 618 amino acid residues. The enzyme acts as an exo-muramidase that removes disaccharide-peptides from one end of the glycan strands (Beachey *et al*., 1981) and it is inhibited by the antibiotic bulgecin A (Templin *et al*., 1992). The combined treatment of *E. coli* cells with this glycopeptide inhibitor and the β-lactam furazlocillin leads to the formation of bulges and enhanced bacteriolysis.

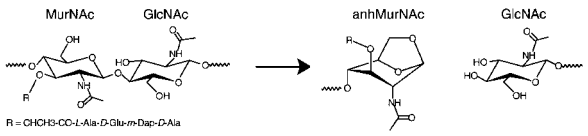

Figure 1. A schematic drawing showing the cleavage and transglycosylation reaction catalysed by lytic transglycosylases.

Considering their unique reaction and intriguing role in murein metabolism, lytic transglycosylases form highly interesting candidates for detailed structural studies. Moreover, there is a growing pharmaceutical interest in these enzymes. Since their activity is directed towards the glycosidic bonds in the glycan strands, they offer a target for structure-based design of novel antibiotics distinctly different from the penicillins and related β-lactam antibacterials, whose main target form the enzymes involved in the synthesis and cleavage of the peptide linkage between the glycan strands (Waxman & Strominger, 1983). A second interest is related to their 1,6-anhydromuropeptide products, which show a number of unusual biological activities in mammals, ranging from the ability to induce sleep (Martin *et al*., 1984; Johannsen, 1993), to stimulate the immune response (Dokter *et al*., 1994) and to properties that are related to the pathogenesis of Gram-negative bacteria like *Neisseria gonorrhoeae* and *Bordetella pertussis* (Melly *et al*., 1984; Cookson *et al*., 1989). The molecular basis for the activities shown by the 1,6-anhydromuropeptides is still not understood.

To increase our knowledge about the peptidoglycan-degrading enzymes, we study the three-dimensional structure of the periplasmic 70 kDa soluble lytic transglycosylase (Slt70) from *E. coli* with X-ray crystallography. The results have already provided information about the overall structure at 2.7 Å resolution and aspects of the catalytic function of this enzyme (Thunnissen *et al*., 1994, 1995a,b). Here we report the refinement and a detailed analysis of its crystal structure at a nominal resolution 1.65 Å. Moreover, the crystal structure of Slt70 complexed with a 1,6-anhydromuropeptide has been determined, revealing the presence of a peptide-binding site at the interface of the α-superhelix and the catalytic domain.

Results

Correctness and quality of the structures

Refinement of models

The native Slt70 model has been refined at 1.65 Å resolution starting from the 2.7 Å resolution

structure previously solved by Thunnissen *et al.* (1994). The high solvent content (about 63 %) and the large amount of electron-rich sulphate ions in the Slt70 crystal prompted the application of a bulk solvent correction to the lower resolution data during the refinement. Furthermore, the anisotropic scattering of the Slt70 crystal suggested the application of an overall anisotropic *B*-factor scaling to F_{calc}. Both corrections dramatically improved the *R*-factors (Table 1) and electron density maps (not shown).

The anisotropy of the Slt70 diffraction data was further analysed by subjecting the final Slt70 model to an anisotropic *B*-factor refinement in SHELXL (Sheldrick & Schneider, 1997) instead of applying an overall anisotropic *B*-factor scaling in X-PLOR. During this procedure the R_{work} and R_{free} refined to 14.4 and 20.1 %, respectively, indicating that the anisotropic *B*-factor refinement resulted in some overfitting. Therefore, the resulting model was only used to extract the general behaviour of the anisotropic atomic *B*-factors, and the *B*-factors from SHELXL were not retained in the final model. The average mean square atomic displacement parameter along the *a*-axis is 0.29 Å^2, which is almost twice the value of the atomic displacement parameters along the *b*-axis (0.16 Å^2) and *c*-axis (0.17 Å^2). The differences between these values agree well with those deduced from the overall anisotropic *B*-factor scaling parameters (Table 1).

Interestingly, the *a*-axis also shows the largest change in cell dimensions upon freezing of the crystal ($a = 80.8$ Å at room temperature and 78.0 Å at 120 K). Analysis of the crystal packing reveals a possible explanation of the observed anisotropy. In the crystal the Slt70 molecules are organised in layers that run parallel to the *ab*-plane and that are stacked along the direction of the *c*-axis. Along the *c*-axis, the layers interact through ridges leading to the formation of large solvent channels parallel to the *b*-axis. The layered packing may well allow some concerted movement along the *a*-axis, by a sliding motion of neighbouring layers, whereas movement along the *b* and *c*-axes is much more restricted due to the presence of more extensive inter-molecular contacts.

The final refinement cycle in X-PLOR resulted in an R_{work} value of 16.8 % for the working set and an R_{free} value of 19.1 % (test set with 10 % randomly selected reflections) for data between 20.0 and 1.65 Å resolution ($|F_{obs}| > 0$). This model was used as a starting model to refine the complex of Slt70 and its 1,6-anhydromuropeptide reaction product (G(anh)MTri), which consists of two sugar residues (GlcNAc and anhMurNAc) with a tripeptide side-chain of L-alanine, D-glutamic acid and *meso*-diaminopimelic acid residues (L-Ala-D-Glu-*m*-Dap). The complex was refined to a final R_{work} of 17.1 % and R_{free} of 19.7 % at 1.90 Å resolution. During the refinement, 5 % of the reflections were set aside for the cross-validation (see Materials and Methods) and no individual *B*-factor refinement was applied, because of the low completeness of the data set. For both models, the last refinement cycle was repeated with all data, which resulted in final *R*-factors of 16.9 % and 17.2 % for the native and complex structure, respectively (Table 1). These models are used in the following analysis.

Quality of the refined models

The native Slt70 model comprises all 618 amino acid residues, 989 water molecules, 13 sulphate ions, seven glycerol molecules and one acetate ion (Table 1). For 26 amino acid residues alternate side-chain conformations were identified. All residues with an alternate side-chain conformation are found at the protein surface; 11 of these residues are involved in crystal contacts. Two glycerol molecules also have alternate conformations and 23 water molecules are bound in alternate positions making at least one hydrogen bond to a neighbouring solvent molecule or amino acid residue. The cross-validated coordinate error of the native model is 0.18 Å as calculated from a Luzzati plot and 0.16 Å as derived from a σ_A plot (Read, 1986). Analysis of the distribution of main-chain dihedral angles shows that of the 552 non-glycine and non-proline residues in Slt70, 522 residues (94.9 %) are in the most favoured regions, while the other 30 residues (5.1 %) are in the additional allowed regions (Morris *et al.*, 1992; Laskowski *et al.*, 1993). The majority of residues (~70 %) are inside the right-handed α-helix region (not shown).

Figure 2(a) and (b) show plots of the real space correlation coefficients for main-chain and side-chain atoms. The average value for the correlation coefficient is 0.98 for the main-chain atoms and 0.94 for the side-chain atoms, showing that the overall fit is good. Asn265 and Asp266 have weak electron density and the lowest correlation coefficients. Side-chain residues with a correlation coefficient lower than 0.75 are all found at the surface of the molecule. Most of them are charged or polar residues located in the N-terminal domain like Arg72, Arg227, Asn265 and Asp266. Another group of residues with weak or poorly defined electron density for side-chain atoms comprises Glu363, Glu365, Gln373, Asp376 and Gln381, which are part of a long surface loop connecting the U and L-domains (see below and Figure 3). In the C-terminal domain only Arg617 has a side-chain real space correlation coefficient lower than 0.80. Disorder in parts of the model, especially for the residues in the surface loop, is also obvious from an analysis of the mean *B*-values per residue (Figure 2(c) and (d)).

The quality of the refined Slt70-G(anh)MTri complex also appeared to be good as judged from the refinement criteria and from an evaluation by PROCHECK (Laskowski *et al.*, 1993). A comparison of the C^α atoms of the Slt70-G(anh)MTri model with those of the native Slt70 model did not reveal any significant changes in the protein structure

Table 1. Statistics of data collection and model refinement

A. *Data collection*								
Slt70	Native				G(anh)MTri			
Wavelength (Å)	0.92				0.92			
Number of measurements	335,588				193,873			
Number of unique data	100,894				57,525			
Resolution limit (Å)	1.65				1.90			
Completeness (last shell in%)	92.3 (75.6)				79.3 (63.7)			
R_{merge} (last shell)	0.048 (0.255)				0.059 (0.148)			
B. *Refinement*								
Resolution range (Å)	20.0-1.65				15.0-1.90			
R-factors in% (No. of refl.)[a]								
	Start final refin.	+bulk. solv. corr.	+anis scaling	Final	Start final refin.	+bulk solv. corr.	+anis scaling	Final
R_{all}	22.7	19.8	17.1	16.9 (97,005)	24.9	21.8	17.3	17.2 (56,504)
R_{work}	22.6	19.6	16.9	16.8 (87,272)	24.8	21.7	17.1	17.1 (53,759)
R_{free}	24.0	21.7	19.2	19.1 (9733)	25.7	23.5	19.6	19.7 (2745)
Bulk solv. model parameters								
Density level (e/Å^3)	0.368				0.340			
B-factor (Å^2)	44.7				34.6			
Anis. scaling (Å^2) parameters								
B_{xx} (U_{xx})	6.3 (0.079)				13.3 (0.169)			
B_{yy} (U_{yy})	−3.8 (−0.048)				−7.0 (−0.089)			
B_{zz} (U_{zz})	−2.5 (−0.031)				−6.3 (−0.080)			
Number of			Average *B*-parameters (Å^2)				Average *B*-parameters (Å^2)	
Main-chain residues	618		15.6		618		21.4	
Side-chain residues	583[b] (26)[c]		18.6		583[b] (24)[c]		24.5	
Water molecules	989 (23)[c]		34.3		874 (3)[c]		38.9	
Sulphate ions	13		49.3		12		61.7	
Glycerol molecules	7 (2)[c]		24.8		5		28.7	
Acetate ions	1		15.6		1		21.3	
GlcNAc	-		-		1		35.5	
anhMurNAc	-		-		1		52.4	
L-Ala	-		-		1		40.4	
D-Glu (*D*-Ala unit)	-		-		1		31.2	
All atoms	6202		20.3		6069		25.8	
RMS-deviations from ideal values[d]								
Bonds (Å)	0.008				0.007			
Angles (°)	1.2				1.2			
Dihedrals (°)	20.0				19.9			
Improper dihedrals (°)	1.32				1.19			

The indicated *R*-factors are the one at the start of the final refinement cycle with subsequent application of a bulk solvent correction and an anistropic *B*-factor scaling. For each data set, the final *R*-factors are found in the fourth column.

[a] *R*-factor = $\Sigma \mid\mid F_{obs} \mid - \mid F_{calc} \mid\mid / \Sigma \mid\mid F_{obs} \mid$. R_{all} is calculated for all reflections in the resolution range. R_{work} and R_{free} are defined for reflections with $|F| > 0$.

[b] Excluding the glycine residues.

[c] The numbers in between brackets indicate the number of alternate (side-chain) positions.

[d] With respect to Engh & Huber parameters (Engh & Huber, 1991).

(root-mean-square deviation of 0.10 Å for 618 C^{α} atoms). The cross-validated coordinate error of the complex model is 0.21 Å as calculated from a Luzzati plot and 0.15 Å as derived from a σ_A plot (Read, 1986). Table 1 summarizes all data collection and refinement statistics.

In the following sections, all the details that describe the conformation of Slt70 were derived from the 1.65 Å native structure, while the 1.90 Å structure of the Slt70-G(anh)MTri complex was used to analyse the binding of the 1,6-anhydromuropeptide.

Overall structure

The overall features of the three-dimensional structure of Slt70 have been described elsewhere (Thunnissen *et al.*, 1994). Briefly, the enzyme is built up of three distinct domains, which are all very rich in α-helices (Figures 3 and 4). In total, nearly two-thirds of all amino acid residues are found in the 37 α-helices and six 3_{10}-helices, while the remaining residues are in the helix-connecting β-turns, γ-turns and loops. The N-terminal domain (residues 1 to 360) contains 22 α-helices (Uα1-

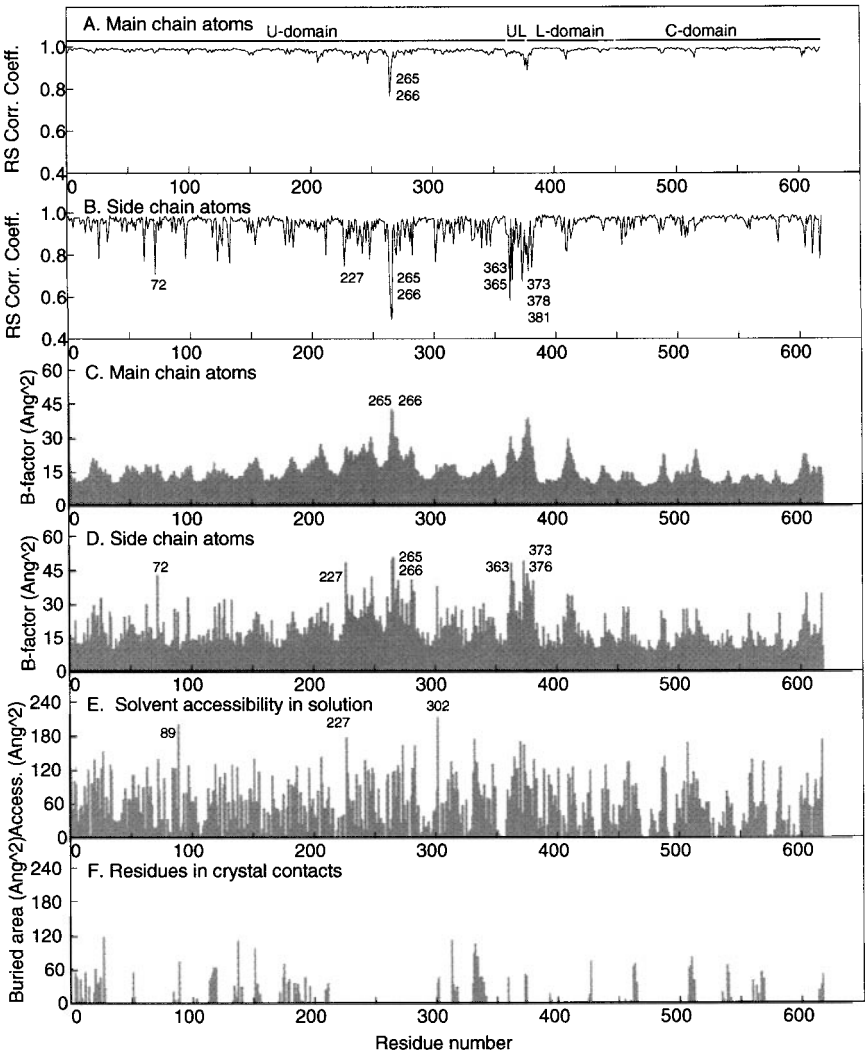

Figure 2. Quality of the final refined model. (a) Real space correlation coefficients for main-chain and (b) side-chain atoms using the final σ_A-weighted $2F_o - F_c$ Fourier map. (c) Plots of the mean *B*-factor for main-chain and (d) side-chain atoms. (e) Solvent accessibility. (f) Buried surface in crystal contacts. Residues that are not well-defined in the electron density are labelled. These residues are mostly found around positions 265-266 and in the UL-loop (UL).

Uα22), packed in an extended, U-shaped conformation. *Via* a long loop of 17 residues, this U-domain is connected to a small linker domain (L-domain; residues 378 to 450) containing two small α-helices (Lα1 and Lα6) and four large α-helices (Lα2-Lα5). Together these first two domains form a closed ring with a large central hole. The C-terminal domain (C-domain; residues 451 to 618) is packed on top of this ring, interacting with part of the L-domain and the C-terminal region of the U-domain. This domain has a globular structure and contains nine different α-helices (Cα1-Cα9). Its overall fold is similar to that of goose-type lysozyme (Thunnissen *et al.*, 1995a), although the homology in amino acid sequence is low. The C-domain contains the active site of Slt70.

In overall schematic terms the Slt70 molecule is best described as an asymmetrically shaped doughnut. It is about 85 Å in height and 75 Å in width, while the thickness varies from ~25 Å for one of the edges of the ring to ~55 Å for the other edge where the lysozyme-like domain is located. The central hole has a diameter varying from 25 Å to about 35 Å.

The U and L-domains

The right-handed α-superhelix

The most striking feature of the Slt70 structure is presented by the ring of α-helices formed by the U-domain and L-domain. Schematics of the α-helical packing are given in Figures 5 and 6. The individual α-helices of the U-domain vary in length from 7 to 17 residues, with an average length of about 12 residues or about three turns (Figure 4). The connecting loops have an average length of five residues, with one residue for the smallest and nine residues for the largest loop. The 22 α-helices

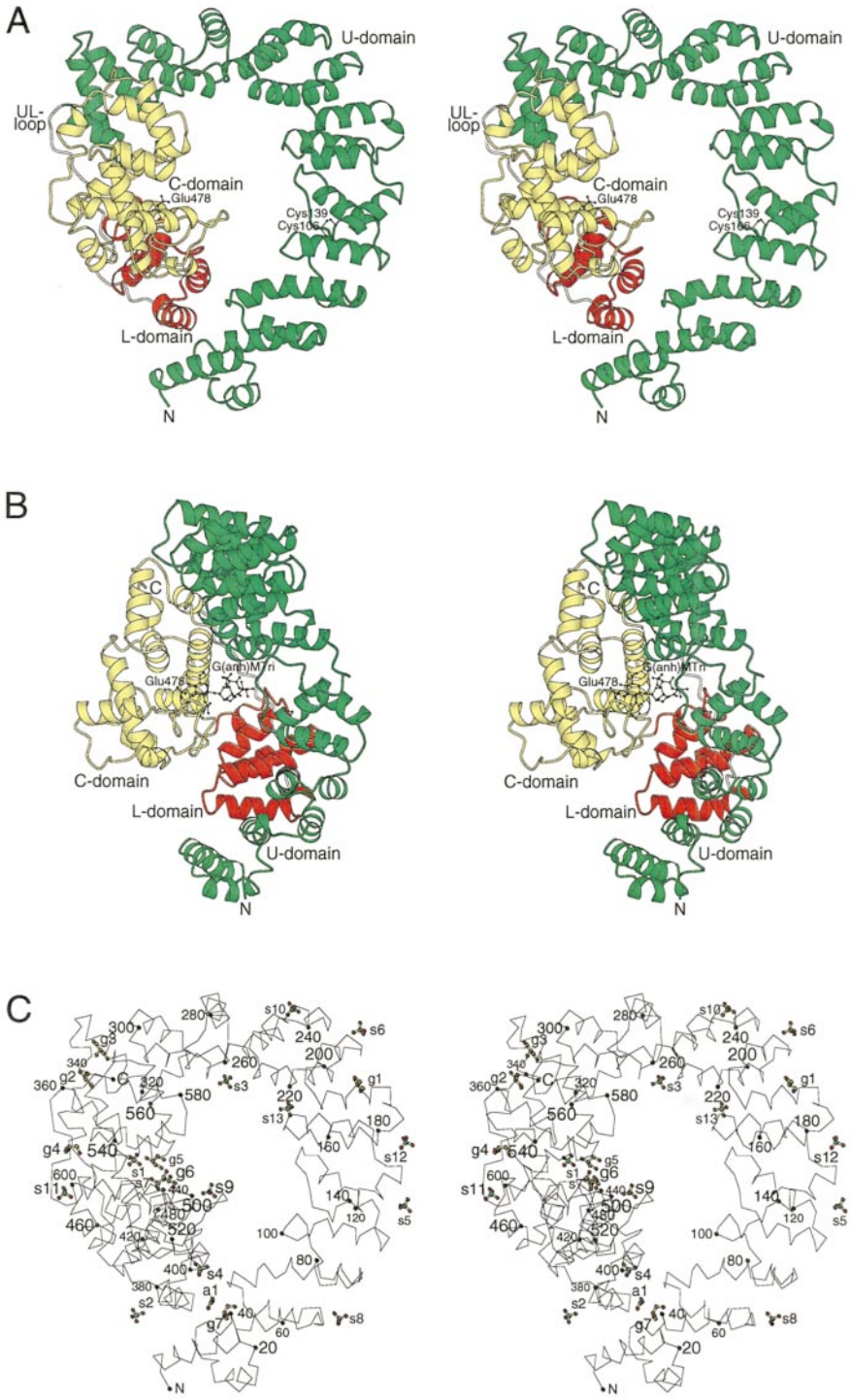

Figure 3. Stereo views of the three-dimensional structure of Slt70. (a) View down the large central hole of the doughnut. (b) Side-on view of the doughnut, with the C-domain at the left. The 1,6-anhydromuropeptide binds at the interface of the U, L and C-domains adjacent to the catalytic acid/base Glu478. The domains are coloured in green for the U-domain, white for the UL-loop, red for the L-domain and yellow for the C-domain. Glu478 and the disulphide bond between Cys106 and Cys139 are indicated in ball-and-stick representation. (c) The C^{α}-trace of Slt70 with sulphate ions (s1-s13), glycerol molecules (g1-g7) and one acetate ion (a1) in an orientation similar to (a).

in the U-domain are roughly located in two curved neighbouring layers. In addition, the helical double-layer is coiled making a twist of about 90°. In this double-layered structure sequentially adjacent helices are connected following an ''up-and-down'' pattern that results in the assembly of a right-handed ''α-superhelix''. The packing of the helices in this ''superhelical'' assembly is such that helix-helix interactions between different layers are all antiparallel, while helix-helix interactions within

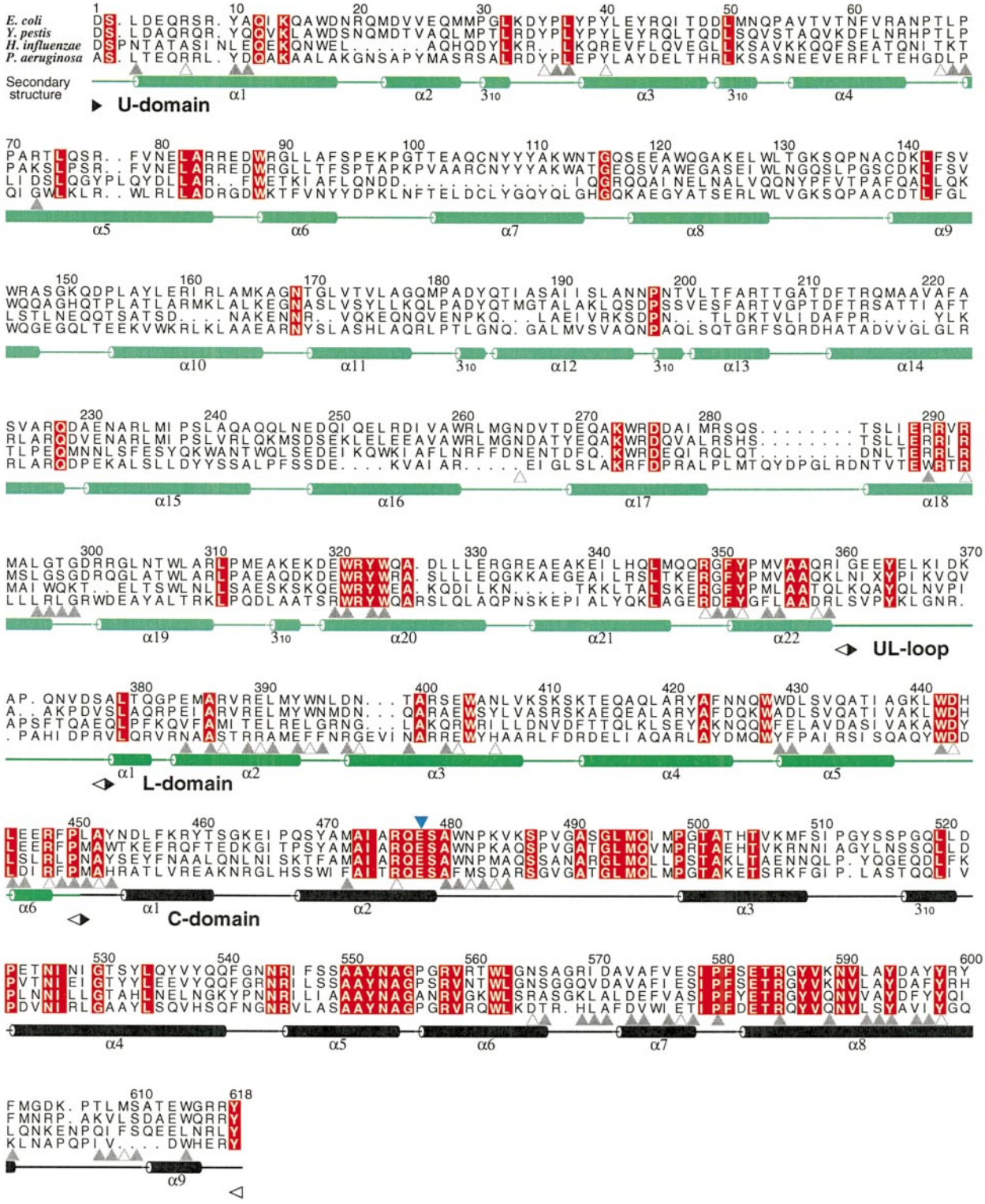

Figure 4. Multiple sequence alignment of Slt70 sequences from *Escherichia coli*, *Yersinia pestis* (62% overall identity), *Haemophilus influenzae* (30% overall identity) and *Pseudomonas aeruginosa* (32% overall identity). Sequences were obtained from the BLAST server at the NCBI (USA) (Altschul *et al.*, 1997). The residue numbering is according to the *E. coli* Slt70 sequence. The blue arrow indicates the *E. coli* Slt70 catalytic acid/base Glu478. The residues of Slt70 that are involved in hydrogen bonding or van der Waals contacts at the domain-domain interfaces are indicated with the open and filled grey arrows, respectively. The alignment was produced with CLUSTAL (Thompson *et al.*, 1994) and ALSCRIPT (Barton, 1993).

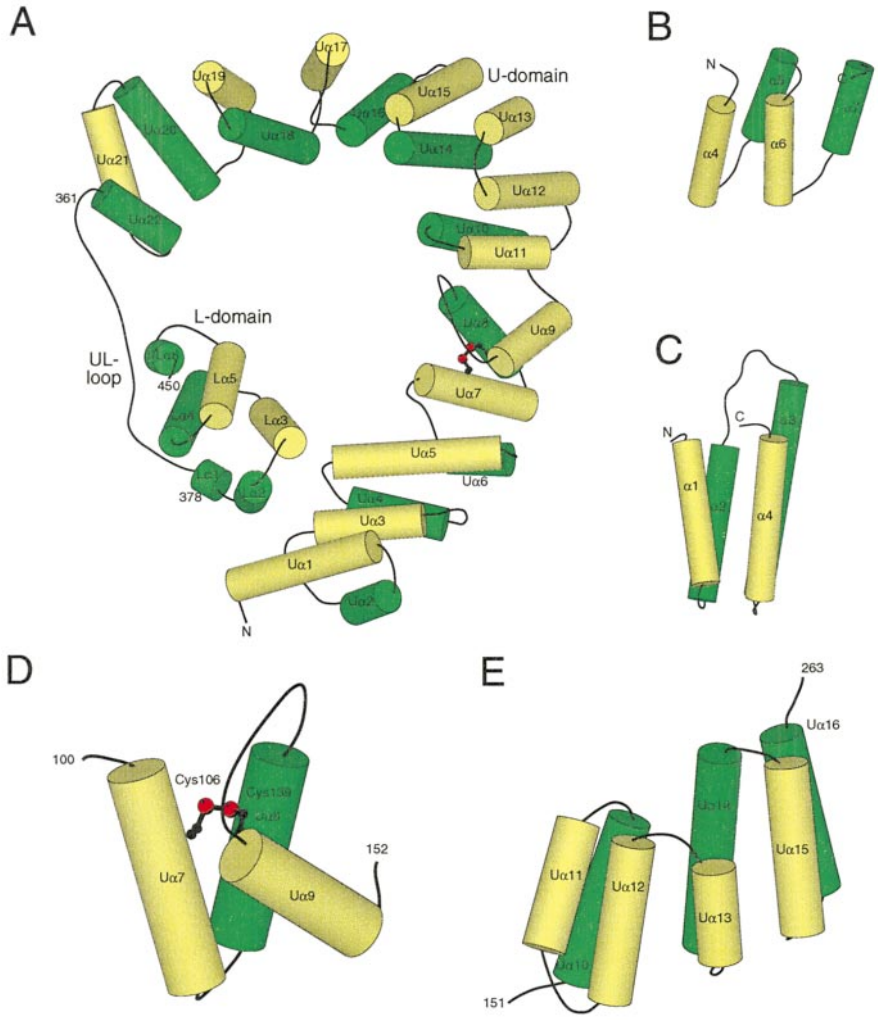

Figure 5. Schematic representations of the arrangement of helices in the U and L-domains of Slt70 (yellow, outer helices; green, inner helices). (a) Overall view of the double-layered superhelical packing. (b) The basic folding unit of the right-handed α-superhelix (protein farnesyltransferase; PDB 1ft1A (Park *et al.*, 1997)). Inter-layer helix pairs (different colours)) are antiparallel, while intra-layer helix-pairs (same colour) are parallel. Interhelical angles are most favourable around 20°. (c) Helical packing in a standard four-α-helix bundle (cytochrome *b*562; PDB 256b (Hamada *et al.*, 1995)). Note that, in contrast to the α-superhelical folding unit (b), all neighbouring helices run antiparallel. (d) Illustration of the distortion in the basic superhelical packing of helices Uα7, Uα8 and Uα9. The N-terminal ends of helices Uα7 and Uα9 are connected through a disulphide bridge. As a result the C-terminal end of Uα9 is pushed away from Uα7, and the helical angle between Uα8 and Uα9 increases to ~60°. Similar distortions of interhelical packing, but without the involvement of disulphides, occur around helix Uα17. The distortions cause a ribbon-like twist in the double-layered superhelix. (e) Illustration of another type of distortion occurring in the middle of the U-domain, which consists of the insertion of helices Uα12-Uα13 as an antiparallel helix pair in the convex, outer layer of the superhelix. This allows for the sharp bend in the U-shaped superhelix.

one layer are all parallel, with the exception of helices Uα11, Uα12 and Uα13 which form antiparallel helix pairs within the same layer (Figure 5(e)).

In the L-domain, the helices Lα2 to Lα5 form a single four-α-helix bundle with a similar double-layered superhelical topology as the helices in the U-domain. The helix-to-helix packing in the U-domain and L-domain of Slt70 differs from that observed in the ''classical'' four-α-helix bundles, for which structurally adjacent helix pairs are all antiparallel (Presnell & Cohen, 1989). However, the right-handed α-superhelix is not unique. Superhelical assemblies of four and five α-helices have been observed in the structures of human annexin V (Huber *et al.*, 1990), and spiny lobster haemocyanin (Gaykema *et al.*, 1984). Also the double-layered α-α-barrel of 12 helices, observed in the structures of the endoglucanase CelD from *Clostridium thermocullum* (Juy *et al.*, 1992), the glucoamylase from *Aspergillus awamori* (Aleshin *et al.*, 1992) and the β-subunit of farnesyltransferase (Park *et al.*, 1997), is an example of an α-superhelical assembly. The best corresponding examples are provided by the crystal structures of the lipovitellin from lamprey yolk (Anderson *et al.*, 1998) and structures of the HEAT and ARM-repeat containing proteins

(Huber *et al*., 1997; Park *et al*., 1997; Kobe *et al*., 1999). What distinguishes Slt70 from most of these other superhelical folds is the absence of obvious internal sequence repeats and the largely extended, non-globular shape of the U-domain. The total accessible surface area of this domain, if separated from the rest of the protein, is ~19,665 Å^2, which is about 35 % larger than the surface area that can be calculated for a globular monomeric protein with a similar molecular weight of ~40 kDa (Janin *et al*., 1988). Only a small area at the N-terminal end of the U-domain packs against the L-domain, and a somewhat larger region at the C-terminal end interacts with the C-domain and L-domain (Table 3, below). The surface area buried by these interdomain interactions comprises only about 15 % of the total accessible surface of the U-domain. In contrast, the superhelical domains in lipovitellin and in the α-subunit of farnesyltransferase are extensively involved in interdomain packing.

Analysis of the helical packing

To better define the structural principles of the α-superhelical fold the characteristics of the interhelical packing were analysed in more detail (Table 2). The packing of two interacting helices is commonly described in terms of the distance of closest approach and the dihedral angle between the two helix axes. The interhelical distances of closest contact in the U and L-domains have values that cover the whole possible range for two interacting helices (Chothia, 1984) with a mean value of 9.8 Å and a standard deviation of 2.2 Å. The line of closest approach is not always located in the middle of the helices, since most of the pairs of adjacent helices form V-shaped structures, with the helical axes tilted away from the interface. The interhelical angles in the U and L-domains show also quite some variation, although there is a clustering of angles around 20° and 40°. The +20° interhelical angle is one of the preferred angles for helix packings observed in several structure analysis studies and is explained by the ''ridges into grooves'' model by Chothia *et al*. (1981). The angle is typical for the helix-packing in the ''classical'' four-α-helix bundle (Weber & Salemme, 1980; Presnell & Cohen, 1989). It seems that the interhelical angles in the U and L-domains of Slt70 are less variable for helices located in opposite layers, than for helices within the same layer. The largest deviations from the +20° interaction angle of interlayer helix pairs are observed around helix Uα7. *Via* a disulphide bond between residues 109 and 139 this helix is covalently connected to the N-terminal end of helix Uα9, distorting the main superhelical packing (Figure 5(d)).

A schematic representation of the extent of the helical interfaces in the different helix pairs is shown in Figure 6. The accessible surface area buried by the interaction of two helices varies between about 25 and 370 Å^2 (Table 2). Helix pairs within the layer at the convex, outer side of the superhelix have in general a less extensive interface compared to the helix pairs at the concave, inner side. This effect is most pronounced at the N-terminal end of the U-domain where helices Uα2-Uα4 are too far apart to interact. In the middle of the U-domain a large disruption of the superhelical packing is prevented by the insertion of helices α12 and α13 as an antiparallel helix pair in the outer layer of the superhelix. On average, about 52 % of the surface of the helices is buried by the helix-helix interactions in the U and L-domains. Not surprisingly, the major part of this buried helical interface is formed by hydrophobic residues with aliphatic and aromatic side-chains: A > L > V > W > I > Y > F (Figure 6(b)). However, also polar residues form a significant part of the interface, in particular arginine residues, which seem to be especially suited for stabilising the superhelical packing. With their long hydrophobic side-chains in core positions the charged headgroups of the arginine residues can still easily reach the surface. In addition, the arginine residues participate in a number of hydrogen bond and salt-bridge interactions that are observed between neighbouring helices. Proline residues form an important factor for tightening and rigidifying the U-domain, especially in the first half where nearly every helix-connecting loop contains one or two of these residues. One of the helices, Uα15, shows a pronounced kink of 40° due to the location of a proline residue in the middle of the helix. Similar kinks in α-helices, caused by an internal proline, have been noted in a number of other α-superhelical proteins (Cingolani *et al*., 1999; Groves *et al*., 1999).

The C-domain

The overall structure of the C-domain resembles the goose-type lysozyme fold (Thunnissen *et al*., 1994, 1995a). It is ellipsoidal in shape with two lobes linked by a long α-helix (Cα4). The active site is found in a deep groove that separates the two lobes. In analogy with the lysozymes and several glycosyl hydrolases (Davies & Henrissat, 1995; White & Rose, 1997) the groove in the C-domain of Slt70 can be divided into six saccharide binding sites, labelled −4 to +2 (Figure 7). The GlcNAc residues of a glycan strand may bind at sites −4, −2 and +1, and the MurNAc residues at sites −3, −1 and +2 (Thunnissen *et al*., 1995a). The site of cleavage is the β(1,4)-glycosidic bond between a MurNAc and GlcNAc residue occupying sites −1 and +1. Based on its equivalence in position to the catalytic glutamic acid in lysozyme, Glu478 at site −1 functions as the general acid in the cleavage reaction catalyzed by Slt70, donating a proton to the oxygen of the scissile glycosidic bond (Thunnissen *et al*., 1995a). In accordance with such a role for residue 478, an E478Q mutation of Slt70 completely abolished activity (Thunnissen *et al*., 1994). The Glu478 side-chain is at the back of site −1, embedded in the protein surface. It is surrounded by a number of conserved, mostly hydro-

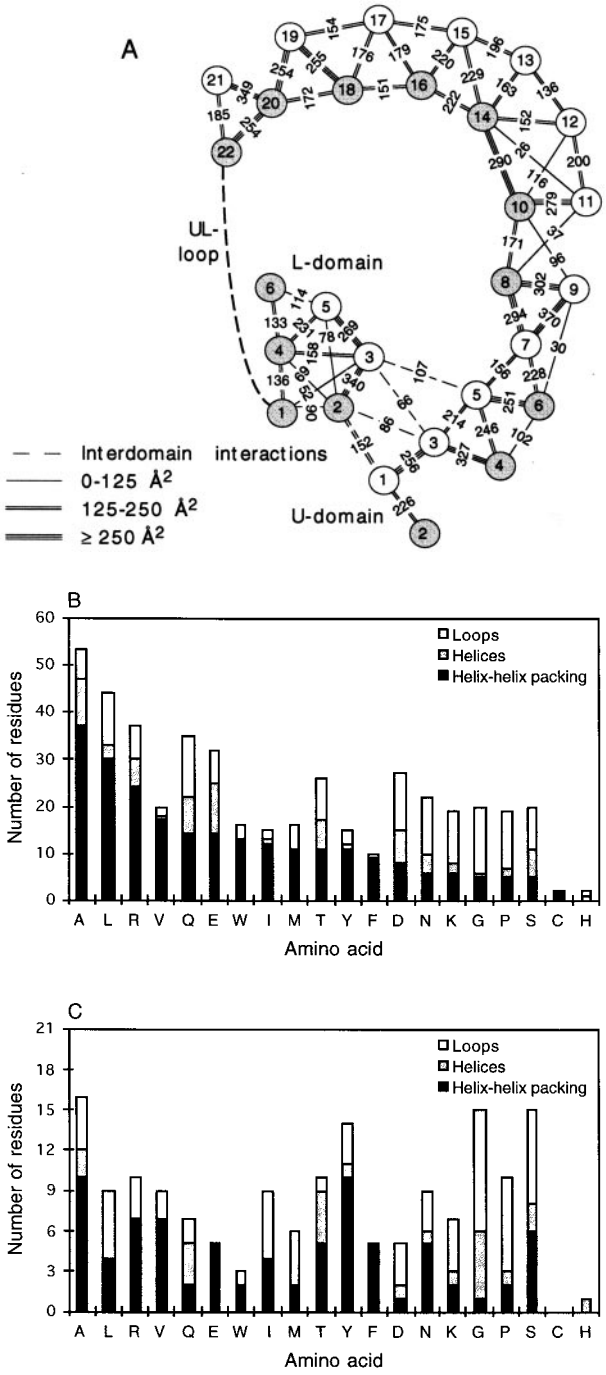

Figure 6. Analysis of the packing interactions between the different helices in the U and L-domains. (a) A schematic representation of the average surface areas buried by the interactions of two neighbouring helices. The averaged buried surface areas (Å^2) were calculated as the loss in accessible surface area, divided by two, on forming one helix-pair out of two isolated helices. (b) Histogram showing the contribution of the different types of amino acids in the U and L-domains (residues 1-450) to the helix -helix interactions. (c) A similar histogram for the C-domain (residues 451-618).

phobic side-chains (Ile474, Met495, Gln496, Tyr552, and Tyr587), while one of its carboxylic O$^{\varepsilon}$ atoms forms a hydrogen bond to the O$^{\eta}$ of Tyr587 (Figure 7). The somewhat buried position of Glu478 in a mostly apolar environment will ensure that the carboxylic group of this residue is mostly protonated under reaction conditions. In addition to its role as general acid, Glu478 may also act as a general base in the second step of the lytic transglycosylase reaction: the formation of a 1,6-anhydrobond in the MurNAc residue at site −1. Crystallographic analysis of the structure of Slt70 complexed with bulgecin A (which binds in sites −2 and −1) led to a proposed mechanism in which Glu478, after cleavage of the glycosidic bond, abstracts a proton from the C6 hydroxyl group of the −1 MurNAc residue. This activates the O6 atom to perform a nucleophilic attack on the C1 atom of the MurNAc oxo-carbonium intermediate (Thunnissen *et al.*, 1995b).

Apart from the glycan strands, Slt70 also needs the peptide cross-links of the peptidoglycan for activity (Romeis *et al.*, 1993). This requirement points to the presence of a specific peptide binding site that participates in the recognition of the substrate. In T4 lysozyme (T4L), which also requires the peptide cross-links for activity, such a binding site has been identified for the peptide that is linked to the MurNAc residue bound at site −1 (Kuroki *et al.*, 1993). In Slt70, the helices Cα6 and Cα7 form a shallow groove on the surface of the upper lobe of the C-domain, very similar to the −1 peptide binding site in T4L (Kuroki *et al.*, 1993; Thunnissen *et al.*, 1995a). The groove is lined with the side-chains of Arg558, Trp562, Asn565, Ser566, Arg569, Ile570, Asp571, Pro580 and Phe581. Most of these residues are conserved in the Slt70 lytic transglycosylases of *E. coli*, *Yersinia pestis*, *Pseudomonas aeruginosa* and *Haemophilus influenzae* (Figure 4). Interestingly, the side-chains of Arg558, Asn565 and Ser566 in Slt70 are at positions equivalent to those of the peptide-interacting residues Arg137, Asn116 and Ser117 in T4L. The other residues in this groove show no similarity to T4L, suggesting that the detailed interactions between the peptides and Slt70 will be different from those in T4L.

Binding of a 1,6-anhydromuropeptide

To further characterize the peptidoglycan-binding groove and to map the residues involved in the binding of peptidoglycan, a Slt70 crystal was soaked in a solution of the 1,6-anhydromuropeptide GlcNAc-anhMurNAc-*L*-Ala-*D*-Glu-*m*-Dap (G(anh)MTri). The compound was obtained as a product of the Slt70-catalyzed cleavage of peptidoglycan (Engel *et al.*, 1992). Difference Fourier analysis revealed that the G(anh)MTri muropeptide was bound at sites +1 and +2. The quality of the difference electron density allowed a clear identification of the binding mode of the G(anh)MTri muropeptide (Figure 8(a)), except for the *D*-Glu side-chain

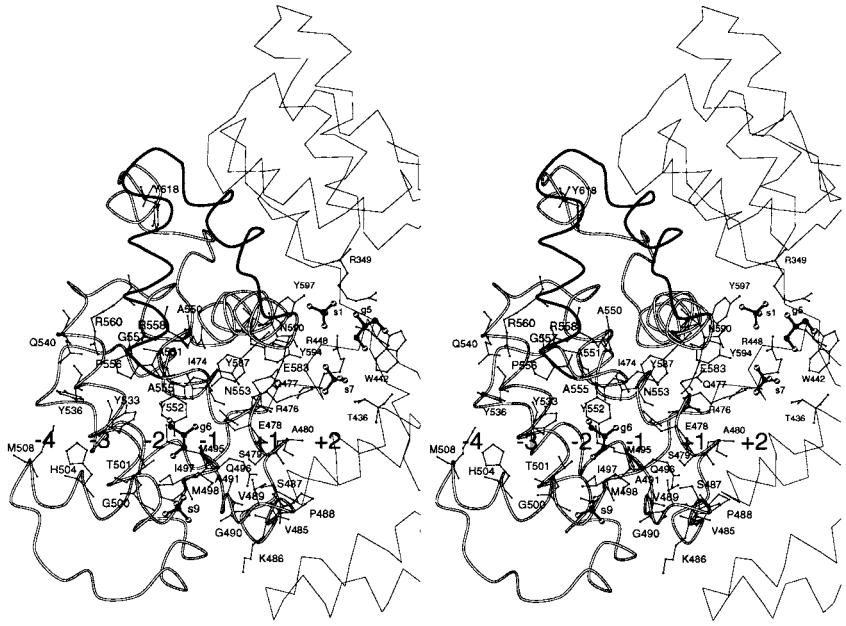

Figure 7. Stereo view of the C-domain in Slt70, showing the amino acid residues that surround the active site groove. Labels −4 to +2 indicate the different sites that may be involved in binding of individual sugar units of the peptidoglycan, based on a comparison with the Slt70-bulgecin A complex and lysozyme-substrate models. The region of the C^{α}-backbone that is highlighted in black defines the putative binding site for the peptide that would be linked to a MurNAc residue bound at site −1.

and *m*-Dap residue for which no electron density was observed, and which thus were left out from the refined model. Details of the muropeptide interactions in the Slt70 peptidoglycan-binding groove are shown in Figures 8(b) and 9. The GlcNAc residue occupies site +1, nearest to Glu478, while the anhMurNAc residue is located in site +2. No muropeptide binding could be observed in sites −4 to −1. Of the two saccharides of G(anh)MTri, only GlcNAc has hydroxyl groups at hydrogen bonding distance to protein atoms. One of these hydrogen bonds occurs between the O4-hydroxyl of GlcNAc and the carboxylic group of Glu478. In addition the backbone carbonyl of Glu478 is at hydrogen bonding distance to the NH of the GlcNAc 2-acetamido group. Two more hydrogen bonds can be formed between the O3-hydroxyl of GlcNAc and the $O^{\varepsilon 1}$ atom of Gln496, and the O6-hydroxyl of GlcNAc and the $N^{\varepsilon 2}$ atom of Gln477.

The sugar ring of the anhMurNAc adopts a distorted $^{1}C_{4}$ chair conformation, as predicted from energy minimization studies (Banic *et al.*, 1994). The $^{1}C_{4}$ chair conformation differs from the normal $^{4}C_{1}$ chair conformation (as observed for GlcNAc at site +1), in that all substituents of the sugar ring are in an axial, instead of an equatorial position. The anhMurNAc residue is only weakly bound to the protein, as indicated by its high average *B*-factor. The conformation of G(anh)MTri is stabilised by two intramolecular hydrogen bonds: one between the O6 atom of the anhMurNAc residue and the amide nitrogen atom of *L*-Ala, the other is a water-mediated hydrogen bond between the 2-acetamido nitrogen atom of anhMurNAc and the 2-acetamido oxygen atom of GlcNAc in site +1. An additional water-mediated hydrogen bond is formed between the *D*-lactyl carbonyl oxygen of the anhMurNAc and $N^{\delta 2}$ of Asn590.

The peptide-binding site is located at the interface of the U, L and C-domains, between the Uα21-Uα22 loop, helices Lα5 and Lα6, and helices Cα2 and Cα8. Most prominent is the salt bridge between the main-chain carboxylate group of *D*-Glu and the side-chain of Arg476. The free *D*-Glu carboxylate group is also at hydrogen bonding distance from the side-chain of Arg448. In the native Slt70 structure, the position of this carboxylate group is occupied by a sulphate ion (Sul707), which makes very similar interactions with Arg448 and Arg476. A second sulphate ion (Sul701), observed in the peptide-binding groove of the native Slt70 structure, interacts with arginine residues 349 and 448 (Figure 8(c)). This sulphate ion is also present in the Slt70-G(anh)MTri structure, and might occupy the binding site for the carboxylate group of the *m*-Dap residue of G(anh)MTri. It could be that the high concentration of sulphate ions in the soaking solution has prevented the binding of the *m*-Dap residue at this site. This would explain the disorder observed in the terminal part of the G(anh)MTri peptide side-chain.

Protein-solvent interactions

Figure 3(c) shows the positions of one acetate ion, seven glycerol molecules and 13 sulphate ions in the native Slt70 model. Six sulphate ions make hydrogen bonds to an amide nitrogen atom near the N-terminal end of α-helices (Sul708 to Uα4, Sul710 to Uα16, Sul703 to Uα18, Sul704 to Lα3, Sul711 to Cα2 and Sul709 to Cα3). One sulphate ion (Sul712) is bound to the amide nitrogen atom at the N-terminal end of a 3_{10}-helix (residues 182-184) and is stabilised by Arg147. All these sulphate

Table 2. Helix-helix interactions in Slt70

Helix pair	D[a] (Å)	H1-H2 contact[b]	Ω (°)[c]	Buried area (Å^2)	Residues involved in helix-helix interactions[d]
U-domain					
Inter-layer					
α1-α2	8.3	C-N	−152.7	226	R9, Q12, I13, A16, W17/M22, V24, V25, M28
α3-α4	11.7	I-I	−161.2	327	P39, E42, Y43, I46/T57, V58, F61
α4-α5	9.7	C-N	−161.0	246	A55, V58, F61, V62, R63/A71, L74, Q75, F78
α5-α6	6.8	C-N	−157.2	251	Q75, F78, V79, L82, A83/W88, G90, L91, F94
α6-α7	8.7	I-I	−121.1	228	W88, L91, L92/N107, Y108, Y110, A111, K112, N114
α6-α9	16.1	N-I	−108.0	30	W88/K141
α7-α8	7.2	C-N	−153.9	294	T102, Q105, C106, Y108, Y109, K112, W113/S118, E120, A121, W122, G124, A125, L128
α8-α9	9.5	I-I	−117.7	302	A121, W122, A125, K126, L128, W129/C139, Leu142, F143, V145, W146
α8-α11	15.0	C-N	−134.6	37	W129/L176
α9-α10	10.6	C-N	−145.0	96	F143, R147/Y157, R160
α10-α11	6.9	C-N	−152.8	279	Y157, R160, I161, A164, M165/T170, L172, V173, V175, L176, A177
α10-α12	11.9	C-C	9.6	116	I161, M165/I191, L194
α11-α14	14.0	N-I	−143.0	26	V173/M217
α12-α14	10.5	C-C	13.6	152	I187, I191, L194/F213, M217, A218, A221
α13-α14	9.3	N-C	−168.5	163	V201, F204/T214, M217, A218, A221, F222, V225
α14-α15	7.9	C-N	−165.9	229	A218, F222, V225, A226, Q228/A230, N232, A233, M236, I237, L240
α15-α16	10.0	N-C	173.9	220	A230, A233, R234, I237, L240, A241/I251, L254, R255, V258
α16-α17	9.0	I-I	−135.2	179	Q252, R255, D256, V258, A259/W274, R275, A278, I279
α17-α18	10.0	C-N	−137.3	176	R275, D276, I279/L287, I288, R291, M294
α18-α19	8.2	C-N	−161.5	255	I288, R291, V292, A295, L296/G303, L304, W307, L308, R310
α19-α20	10.8	I-I	−130.7	254	R301, L304, N305, L308/W321, W324, Q325, D327, L328, E331
α20-α21	7.3	C-N	−154.0	349	D319, R322, Y323, Q325, A326, L329, L330/E337, A338, K339, I341, L342, Q344, L345
α21-α22	8.0	I-I	−136.4	185	L342, L345, M346/P353, A356, A357, R359
Intra-layer					
α1-α3	11.2	N-N	17.7	256	Y10, I13, K14, W17, D18/Y40, L41, R44, Q45, D48
α3-α5	10.8	N-N	14.8	214	Y40, Y43, I46, T47/P69, P70, T73, L74, R77
α4-α6	10.4	I-C	−17.1	102	A55, V58, T59, R63/F94
α5-α7	9.1	I-I	38.0	156	S76, V79, N80, A83/E103, A104, N107
α7-α9	8.1	I-N	41.3	370	C106, N107, Y109, Y110, W113/C139, K141, L142, V145
α8-α10	9.7	C-C	27.3	171	W129/A156, Y157, R160
α10-α14	9.6	C-I	12.1	290	L158, I161, R162, M165, K166/F213, Q216, M217, V220, A221
α11-α12	8.0	I-I	−156.1	200	T170, V173, T174, A177, G178/A188, I191, I192, A195
α12-α13	9.5	C-N	−167.0	136	A190, I191, L194/V201, F204
α13-α15	9.7	N-N	−2.8	196	V201, L202, A205, R206/M236, S239, L240, A243
α14-α16	8.5	C-C	−19.0	222	R215, A219, F222, A223, A226/Q250, E253, L254, I257, V258
α15-α17	11.2	N-N	45.0	175	E231, R234, I237/E270, Q271, W274
α16-α18	10.6	I-I	30.9	151	D256, A259, W260/S286, L287, R290
α17-α19	11.0	C-C	24.8	154	D276, I279, M280/W307, R310
α18-α20	12.3	I-I	43.3	172	E289, V292, R293, L296/E320, W321, W324
α20-α22	8.7	N-N	18.0	254	D319, E320, Y323, W324, D327, L330/Y352, P353, V355, R359
L-domain					
Inter-layer					
α1-α3	11.9	I-I	149.2	52	L379/L407
α2-α3	8.0	C-N	−156.4	340	E384, M385, R387, V388, L391, M392/D397, T399, A400, E403, W404, N406, L407
α2-α5	10.6	C-N	136.4	78	V388, M392/D430, L431
α3-α4	10.2	C-N	155.0	158	W404, L407, V408/Q416, L419, A423
α4-α5	7.4	C-N	−165.9	231	Q416, L419, A420, A423, F424/W429, L431, S432, A435, T436, A438
α5-α6	7.7	I-C	−134.8	114	S432, V433, T436/E447, R448
Intra-layer					
α1-α2	4.0	C-I	−53.3	90	L379, T380, Q381/P383, M385
α1-α4	9.9	N-I	−48.0	136	L379, T380/E415, L419, Y422
α2-α4	12.7	I-C	−31.3	69	M385/L419, Y422
α3-α5	9.7	I-I	−29.7	269	D397, A400, R401, W404, A405, V408/D430, L431, Q434, A435, A438
α4-α6	9.9	I-I	45.4	133	A420, R421, F424/E446, E447
Inter-domain					
Uα1-Lα2	12.2	I-I	−62.4	152	L3, R7/R389, E390, Y393
Uα3-Lα2	9.3	N-I	−77.9	86	Y40/R387, L391
Uα3-Lα3	13.7	N-I	112.5	66	Y40/T399, E403
Uα5-Lα3	7.8	N-I	99.4	107	P69, R72/E403, N406

Helix pair	D[a] (Å)	H1-H2 contact[b]	Ω (°)[c]	Buried area (Å^2)	Residues involved in helix-helix interactions[d]
C-domain					
α1-α2	8.4	I-N	126.6	201	N454, F457, K458, T461/Q468, A471, M472, A475
α1-α4	9.7	I-I	−39.2	254	L456, F457, R459, T460, T461/P523, E524, I527, N528, T531
α2-α4	10.3	I-I	116.4	129	Y470, A471, I474/T531, L534, Y538
α2-α5	12.3	I-I	−35.6	173	Y470, I474, E478/R545, S548, S549, Y552
α2-α8	8.0	I-I	130.6	410	S469, Y470, M472, A473, I474, R476, Q477, E478/Y587, N590, V591, Y594, D595, Y598, R599
α3-α4	9.9	I-I	71.0	265	T501, A502, T505, V506, M508, F509/I529, S532, Y533, Y536
α4-α5	9.1	I-I	122.7	215	G530, Y533, L534, V537, Y538/R545, S548, A551, Y552
α4-α6	11.8	I-N	−26.4	73	Y533, V537, Q540/P556, R560
α5-α6	6.0	C-N	130.3	212	F547, A550, A551, A554/P556, R558, V559, W562, L563
α5-α7	10.6	N-N	12.1	112	I546, F547/A572, F575, V576
α5-α8	9.1	I-I	129.2	333	R545, I546, S549, A550, Y552, N553, A554/E583, T584, Y587, V588, V591, L592, D595
α5-α9	8.7	N-I	−79.7	80	R545/E613
α6-α7	11.3	I-I	121.8	89	W562, L563, S566/F575
α6-α8	13.1	I-I	−99.6	38	W562/T584
α7-α8	6.9	C-N	−134.0	146	V576, E577/R585, V588, K589
α7-α9	6.0	N-C	72.4	69	A572, V573/E613, W614
U and C-domain					
Uα18-Cα6	8.0	C-C	−72.6	32	G297/N565, S566
Uα18-Cα7	8.1	I-I	−139.7	169	R293, L296, G297/A574, E577, S578
Uα18-Cα8	12.5	I-N	67.7	65	R293/R585
Uα20-Cα7	12.0	I-I	−145.3	145	E320, W321, Y323, W324/V573, A574, E577
Uα22-Cα7	11.0	C-N	−162.9	132	F351, Y352, V355/V573, V576, E577
Uα22-Cα8	8.7	N-I	63.0	189	F351, Y352, M354/K589, L592, A593, A596, Y597
Uα22-Cα9	12.5	I-I	−91.9	116	V355, Q358, R359/W614
L and C-domain					
Lα5-Cα2	11.3	I-C	−60.8	58	V433/R476
Lα6-Cα2	10.9	C-I	88.9	52	R448/R476
Lα6-Cα8	10.3	C-I	−111.9	146	L445, E446/Y597, F601

[a] D = shortest interaxial distance of two interacting helices.
[b] The closest approach between the interacting helices is indicated of the first (H1) and the second helix (H2) with either C (C terminus of the helix), N (N terminus of the helix) or I (Intermediate).
[c] Ω = the interaxial angle of two interacting helices.
[d] The residues after "/" belong to the second helix. The underlined amino acid residues make H-bonds within 3.2 Å to the other helix.

ions are stabilised by helix macrodipoles (Hol, 1985). One of the six helix-bonded sulphate ions (Sul711) is also contacting Arg302 of a neighbouring molecule.

Three sulphate ions are bound to arginine side-chains from two different domains. Sul702 is bound at the interface between the N-terminal end of the U-domain and the L-domain and it makes salt bridges to Arg7 and Arg389. The two other sulphate ions are found in a deep groove made up of residues of the C-domain and the α-superhelix. Sul701 forms salt bridges with Arg349 of the U-domain and Arg448 of L-domain, while Sul707 is bound to Arg448 of the L-domain and Arg476 of the C-domain.

Two glycerol molecules are found at crystal contacts (Glc901 and Glc902). Two other ones (Glc905 and Glc906) are observed in the peptidoglycan-binding groove of the native Slt70 structure, but are absent in the Slt70-G(anh)MTri complex. Glc906 is bound at site −2 in a position where the 2-acetamido group of the GlcNAc residue of bulgecin A binds (Thunnissen *et al.*, 1995b). The other one (Glc905) is found at site +2 at the interface of the U-domain and L-domain. It interacts with Trp442 from the L-domain through hydrophobic and van der Waals contacts and forms hydrogen bonds to Arg349 and sulphate ion Sul701. Two additional glycerol molecules are found at domain interfaces. One of these (Glc904) is bound at the interface of the U and C-domains, while the other (Glc907) is at the interface between the N-terminal end of the U-domain and the L-domain. Glc907 is in van der Waals contact with the single acetate ion (Act801) in the structure, which is bound in a hydrophobic pocket at the interface of the U-domain and L-domain formed by the side-chains of Tyr40, Leu396, Thr399, Leu391 and the backbone of Glc907. One carboxylate oxygen of the acetate ion is at hydrogen bonding distance from the hydroxyl group of Tyr10 and the amino-group of Lys14. The other carboxylate oxygen can be hydrogen-bonded to Thr399 and Lys14 *via* two water molecules.

Domain interactions

The modular appearance of Slt70 suggests that the C-domain may be active on its own. However, attempts to produce active deletion mutants of

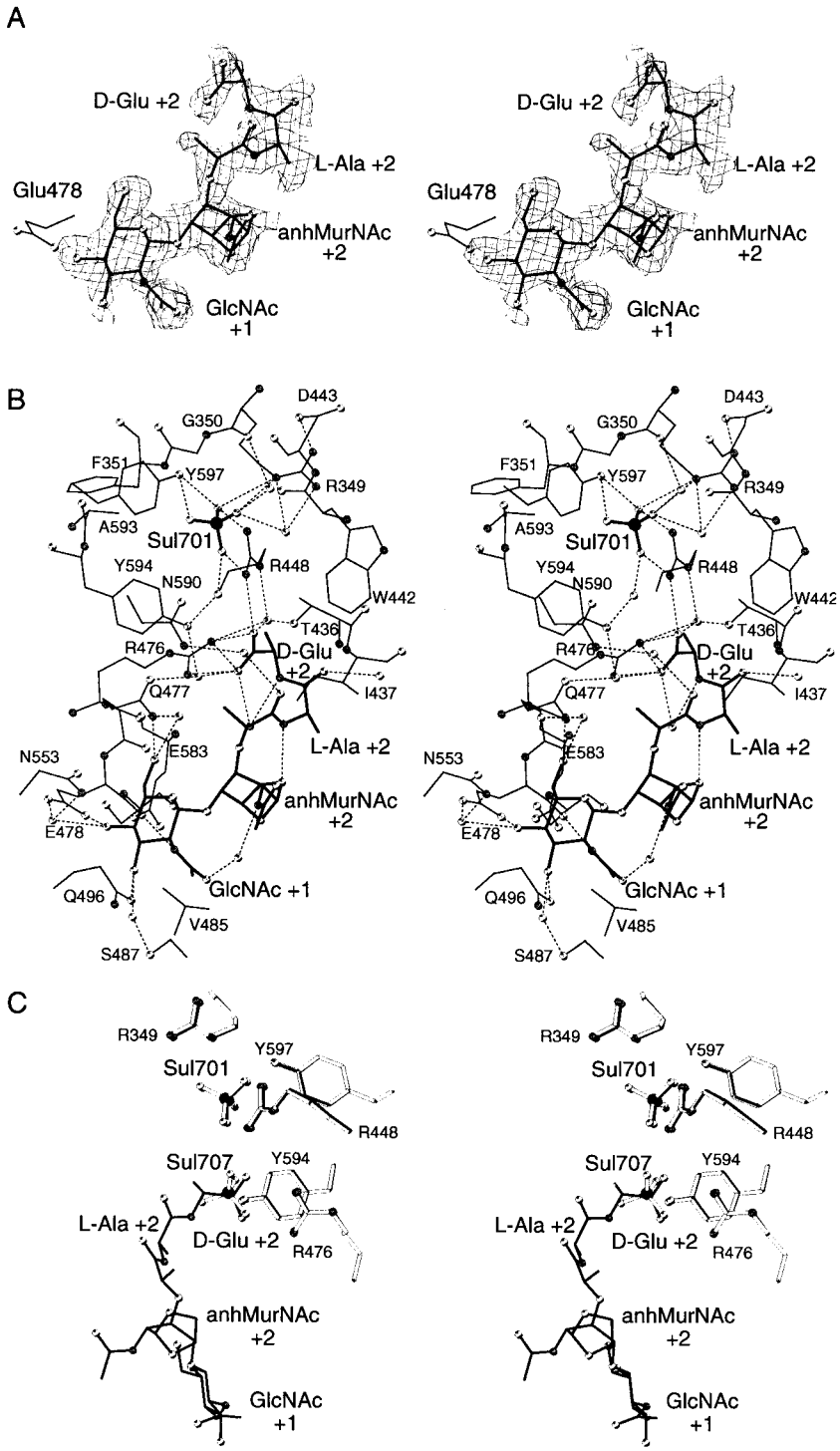

Figure 8. The binding of the 1,6-anhydromuropeptide to Slt70. (a) Stereo view of a simulated annealing omit $F_o - F_c$ electron density map of the G(anh)MTri muropeptide. The map is contoured at 1.8σ. (b) Stereo diagram showing the refined structure of the 1,6-anhydromuropeptide in the +1 and +2 sites of Slt70. Inferred hydrogen bonds are shown as thin dotted lines. Oxygen atoms are shown in white, nitrogen atoms in grey and sulphate atoms in large dark grey circles. (c) Superposition of the G(anh)MTri muropeptide (thick black sticks) on the sulphate ions found in the +2 peptide site of the native Slt70 structure (thick white sticks).

Slt70 missing the first 278, 365 or 449 residues, respectively, failed due to the inability of the mutants to fold properly (Dijkstra, 1997). In order to understand this result, the packing of the three different domains in the Slt70 doughnut was analysed in more detail.

U-L interface

The interface of the U-domain and L-domain is responsible for the closure of the α-superhelical ring. It is formed by the packing of the N-terminal parts and preceding loops of helices α1, α3 and α5 of the U-domain and helices α2 and α3 of the L-domain. The interface buries 594 Å^2 of the solvent-accessible surface area of the U-domain (buried area in the L-domain is 585 Å^2). Atomic contacts in the interface are listed in Table 3. About 60 % of the buried interface is hydrophobic. There are seven hydrogen bonds between side-chain atoms and one hydrogen bond between a main-

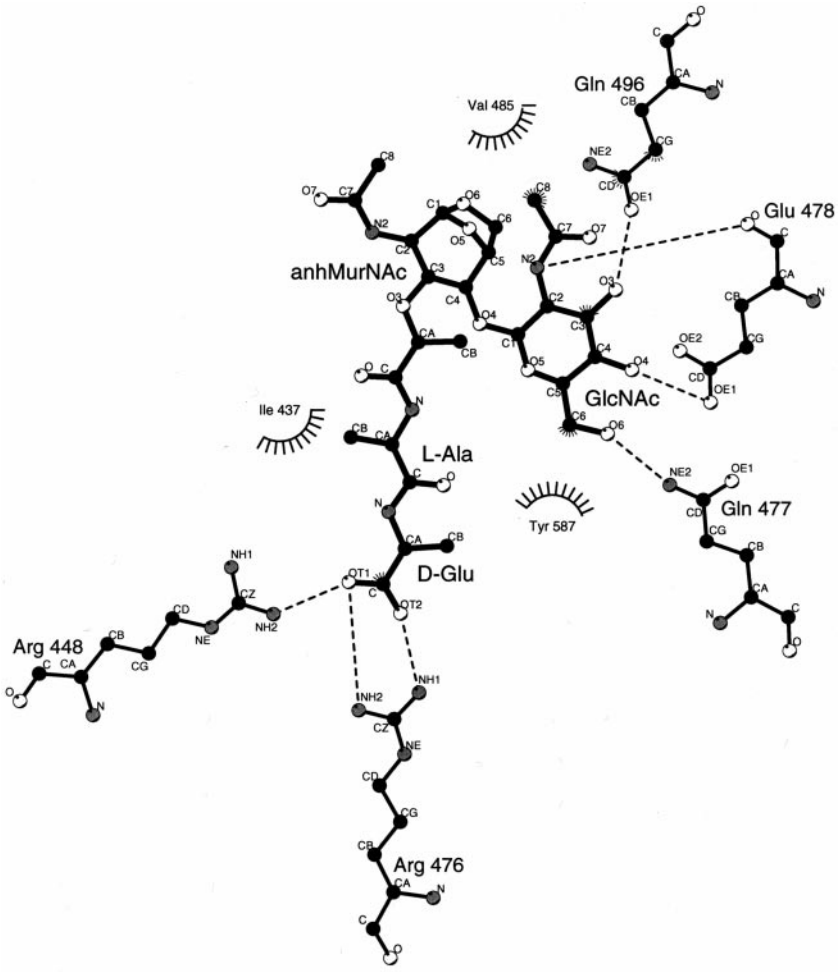

Figure 9. A schematic showing the muropeptide interactions with the Slt70 residues. This picture was produced with LIGPLOT (Wallace *et al.*, 1995).

chain and a side-chain atom. Three water molecules mediate hydrogen bonds in the interface. Furthermore, one sulphate ion, one acetate ion and one glycerol molecule are involved in the hydrogen bonding network of the interface. Central residues in the interface are Arg7 and Glu390, which are involved in a number of polar and apolar contacts with different residues.

Besides the N-terminal part, also the C-terminal part of the U-domain interacts with the L-domain. This interface buries 111 Å^2 of the solvent accessible area of the U-domain and 83 Å^2 of the L-domain. Arg349 is the only residue in the C-terminal U-domain that interacts with the L-domain making one salt bridge with Asp443 and several van der Waals interactions.

U-C interface

The U-C interface is the most extensive of the three domain interfaces. It is formed through the packing of helices in the C-terminal part of the U-domain (Uα18, Uα20 and Uα22) with three helices in the C-terminal lobe of the C-domain (Cα6, Cα7, Cα8). It buries 921 Å^2 of the accessible surface area of the U-domain (853 Å^2 in the C-domain). The majority of contacts are of an apolar nature. Especially the interface between helices Uα22 and Cα8 is highly hydrophobic. Gly297 and Gly299 in the loop between Uα18 and Uα19 are closely packed to helix Cα7. Twelve hydrogen bonds can be identified that cross the interfaces between Cα7, Uα18 and Uα19, with five being mediated through a water molecule (Table 3). Two of the hydrogen bonds are involved in a salt bridge between Arg293 and Glu577.

L-C interface

Apart from the covalent link through the polypeptide backbone, the L and C-domains are connected through an interface that is mainly formed by the N-terminal parts of helices Lα3 and Lα5 and a loop in the C-domain that connects the Cα2 helix with the first β-turn of the floor of site −1. With relatively few amino acid residues a tight, mostly hydrophobic interface is created with 655 Å^2 of the accessible surface of the L-domain buried, and 611 Å^2 of the C-domain. The L-C interface is located near sugar-binding site +2.

U-L loop

The loop that connects the U-domain to the L-domain forms a remarkable feature of the Slt70 structure. With its entire length of 17 residues the

Table 3. Interdomain interactions in Slt70

H-bonds					#l Van der Waals contacts	
Residue	Atom	Residue	Atom	Distance (Å)[a]	Residue	Residue
U-domain		L-domain			U-domain	L-domain
Arg7	N^{ε}	Glu390	$O^{\varepsilon1}$	2.8	Leu3	Arg389, Glu390
	$N^{\eta2}$		$O^{\varepsilon2}$	3.0	Arg7	Arg389, Glu390, Tyr393, Trp394
Tyr35	O^{η}	Glu390	$O^{\varepsilon1}$	2.5	Tyr10	Trp394
		Trp394	$N^{\varepsilon1}$	2.9	Ala11	Trp394
Tyr40	O^{η}	Glu403	$O^{\varepsilon2}$	2.6	Tyr35	Glu390, Trp394
Thr67	$O^{\gamma1}$	Arg387	$N^{\eta2}$	2.9	Pro36	Ala386, Arg387, Glu390
	O	Asn406	$N^{\delta2}$	3.2	Leu37	Arg387, Glu390, Leu391, Trp394
Arg349	$N^{\eta1}$	Asp443	$O^{\delta1}$	3.1	Tyr40	Arg387, Leu391, Thr399, Glu403
Water-mediated H-bonds					Thr67	Glu384, Arg387, Asn406
Tyr40	O^{η}	Thr399	O	2.8/2.8	Leu68	Arg387, Glu403
Asp4	$O^{\delta1}$	Tyr393	O^{η}	2.9/3.0	Pro69	Ser402, Glu403, Asn406
Arg7	$N^{\eta1}$	Tyr393	O^{η}	3.0/3.0	Arg72	Asn406
Thr67	$O^{\gamma1}$	Arg387	$N^{\eta1}$	3.2/2.8	Arg349	Trp442, Asp443, Leu445, Arg448
U-domain		C-domain			U-domain	C-domain
Asn265	$N^{\delta2}$	Asn565	$O^{\delta1}$	2.7	Asn265	Asn565
Arg293	$N^{\varepsilon2}$	Glu577	$O^{\varepsilon2}$	2.9	Arg290	Pro580
			O	3.0	Arg293	Glu577, Ser578, Arg585
	$N^{\eta2}$		$O^{\varepsilon2}$	2.8	Leu296	Ile570, Ala574, Glu577, Ser578
Tyr352	O^{η}	Glu577	$O^{\varepsilon1}$	2.7	Gly297	Asn565, Ser566, Arg569, Ile570, Ala574, Ser578
Gln358	$O^{\varepsilon1}$	Met609	N	2.9	Thr298	Arg569, Ile570
	$N^{\varepsilon2}$		O	3.0	Gly299	Arg569, Ile570
Water-mediated H-bonds					Glu320	Glu577
Glu320	$O^{\varepsilon1}$	Lys589	N^{ζ}	2.9/2.8	Trp321	Glu577
Tyr323	O^{η}	Asp571	$O^{\delta2}$	2.6/2.8	Tyr323	Val573
Asp327	$O^{\delta1}$	Asp571	$O^{\delta2}$	3.2/2.8	Trp324	Asp571, Val573, Ala574, Glu577
Gly350	N	Tyr597	O^{η}	2.9/2.7	Arg349	Tyr597
Arg290	N^{ε}	Pro580	O	3.1/2.8	Arg350	Tyr597
					Phe351	Val576, Lys589, Leu592, Ala593, Leu608
					Tyr352	Val573, Glu577, Lys589
					Met354	Ala593, Ala596, Tyr597, Leu608
					Val355	Val573, Leu608, Trp614
					Gln358	Thr607, Leu608, Met609, Ser610, Trp614
					Arg359	Trp614
L-domain		C-domain			L-domain	C-domain
Asn398	$O^{\delta1}$	Asn482	$N^{\delta2}$	3.0	Asn395	Lys484
Asn398	$N^{\delta2}$	Lys484	O	3.1	Asp397	Asn482, Pro483, Lys484
Arg448	O	Arg476	N^{ε}	2.8	Asn398	Asn482, Lys484, Val485
Pro450	O	Ala452	N	2.8	Trp429	Leu451, Ala452, Tyr453, Trp481
		Tyr598	O^{η}	2.8	Asp430	Ala480, Trp481, Asn482, Pro483
Water-mediated H-bonds					Val433	Arg476, Ala480, Trp481,
Asp430	O	Ala480	O	2.8/2.8	Leu445	Tyr597, Phe601
Thr436	$O^{\gamma1}$	Arg476	$N^{\eta2}$	2.8/3.2	Glu446	Phe601
Arg448	N^{ε}	Arg476	$N^{\eta2}$	2.9/3.2	Arg448	Arg476
Asp430	N	Trp481	O	2.9/2.8	Phe449	Leu451, Arg476, Tyr594, Tyr597, Tyr598, Phe601
					Pro450	Leu451, Ala452, Met472, Trp481, Tyr598, Phe601

[a] A distance cut off of 3.2 Å for a H-bond was applied. If two distances are printed, the H-bond is mediated *via* a water molecule. The first H-bond refers to the distance between the first mentioned residue and the water molecule, while the second distance refers to the distance between the water molecule and the last named residue.

loop is running over the protein surface with the first 16 residues (residues 361 to 376) folded in an extended β-conformation. After residue 364 the loop leaves the surface of the U-domain, passes shortly over the surface of the C-domain, and wraps around the L-domain with residues 366 to 377 interacting with helices Lα6, Lα4 and Lα1 and the loop following helix Lα5. The U-L loop is anchored to the protein surface mainly by the burying of four hydrophobic residues (Tyr364, Leu366, Ala371, and Val375). Residues Glu363, Glu365, Lys367, Lys370, Gln373, and Asn374 have side-chains that are fully exposed to solvent, contributing to the large solvent-accessible surface area of the loop (1,324 $Å^2$). The high solvent exposure probably causes the loop to be very mobile explaining why the electron density in this region is weak for the side-chains. Apart from the outer ends the loop is not involved in crystal contacts.

The analysis of the Slt70 interdomain packing thus shows, apart from the presence of salt bridges and hydrogen bonds, an extensive, largely hydrophobic surface area that is buried between the C-domain and the two superhelical domains. If the

U and L-domains were to be removed from Slt70, the resulting increase in surface hydrophobicity would have a destabilising effect, explaining why the U and L-domains are important for a proper folding and stability of an active C-domain of Slt70.

Discussion

Origin and function of the α-superhelix

The α-superhelical U-domain forms the most remarkable feature of the Slt70 structure. The non-globular fold of this domain is not commonly observed for a single polypeptide chain. Stabilisation of the fold seems nevertheless to arise from the same principles that are believed to function in globular proteins. The main stabilisation comes from the burying of an extensive, though narrow core of mainly apolar residues. Alanine and leucine residues are found most often in the buried core of the α-superhelix, a preference that is typical for four-α-helix bundles (Paliakasis & Kokkinidis, 1992). With its non-globular shape and supersecondary folding the α-superhelix in the U-domain of Slt70 resembles other topologies of secondary supercoils (Baumann *et al*., 1993; Kobe & Deisenhofer, 1993; Yoder *et al*., 1993). An important difference, though, is the level of organisation of the secondary structure building blocks, which is much less regular in the α-superhelix of Slt70. This explains why no obvious periodic sequence motif can be found that determines the supersecondary fold, whereas the other folds clearly have internal sequence identities or similarities that correspond to the structural pseudo-symmetry. Furthermore, no obvious similarities can be found when the sequence of the α-superhelix in Slt70 is compared to that of the structurally related α-superhelix in lipovitellin, which also lacks internal repeats. In fact, even among the Slt70s from four different bacteria only 44 out of the 450 residues are conserved in the α-superhelix (Figure 4). In contrast, the catalytic C-domain of the Slt70s shows 49 conserved residues out of the 168 amino acids. The helices Cα18, Cα20 and Cα22 of the α-superhelix show some conserved stretches of amino acid residues, which interact with residues of the catalytic C-domain (Tables 2 and 3). These interactions may be important to stabilise the C-domain. Due to the low sequence conservation in the superhelical domains it is not possible to draw conclusions on the evolutionary origin of this fold and to tell whether or not it arose from gene duplications of a single building block, such as for instance a four-α-helix bundle. Of course, it could be that during the course of evolution many of the sequence identities have been lost in concert with changes in the helical packing.

Another intriguing question concerns the function of the U and L-domains. Besides their importance for the proper folding and conformational stability of an active C-domain, the U and L-domains might be important for the interaction of Slt70 with peptidoglycan. It has been shown that *in vivo* Slt70 is tightly attached to the murein layer of the cell wall (Walderich & Höltje, 1991). The high affinity might be explained by the presence of additional murein-binding sites distinct from the active site groove in the C-domain. The presence of a substrate-binding site separate from the catalytic site is quite common in enzymes that work on complex polymeric substrates and it has been observed in several oligosaccharide-metabolising enzymes, like cellulases, xylanases and CGTases (Meinke *et al*., 1991; Lawson *et al*., 1994). However, our crystallographic studies have so far not revealed any murein-binding sites at the U and L-domains away from the C domain.

Affinity-chromatography studies have suggested that Slt70 binds to murein-synthesising and murein-degrading enzymes of *E. coli* forming a murein-metabolising complex (Höltje, 1996; von Rechenberg *et al*., 1996). The α-superhelical ring of Slt70 may be responsible for the interaction with these proteins, by analogy with the superhelical domains of farnesyltransferase (Park *et al*., 1997), lipovitellin (Anderson *et al*., 1998) and importin α (Kobe, 1999). However, it is difficult to infer from the Slt70 structure and the low sequence homology among the four Slt70s, which regions could specifically be involved in protein-protein interactions. Further research will be necessary to conclusively establish the existence of such binding sites in Slt70.

Peptide-binding and exo-muramidase activity

The crystallographic analysis of the Slt70-G(anh)MTri complex reveals the presence of a specific binding site for the peptide side-chain linked to the anhMurNAc saccharide at site +2. This peptide-binding site consists of residues that are conserved in the Slt70s from different bacterial species (Arg349, Phe351, Trp442, Arg448, Arg476, Asn590, Tyr594 and Tyr597; Figure 4), underlining the importance of this site for the function of the enzyme. Thus, Slt70 is the second muramidase for which a specific binding site for the peptide moieties of the peptidoglycan has been identified, the only other example being T4L in which binding was observed for a peptide linked to the saccharide bound in site −1. No binding was observed for the 1,6-anhydromuropeptide at sites −2 and −1 of the Slt70 peptidoglycan-binding groove, suggesting that the affinity for the 1,6-anhydromuropeptide product is much lower in these sites than in sites +1 and +2. In contrast, the inhibitor bulgecin A was observed to bind in sites −2 and −1 (Thunnissen *et al*., 1995b).

The high affinity of sites +1 and +2 for the 1,6-anhydromuropeptide reaction product of Slt70 may have two important implications for the function of Slt70. Firstly, such high affinity may be required to keep the GlcNAc residue bound in site +1 during the two steps of the lytic transglycosyla-

tion reaction: the cleavage of the glycosidic bond and the formation of the 1,6-anhydrobond in the MurNAc residue. In hen egg white lysozyme, the GlcNAc residue in site +1 is exchanged with a water molecule after the cleavage reaction. The water molecule is then activated by the active site glutamate, and it attacks the C1 atom of the MurNAc residue in site −1. In contrast, after the cleavage of the glycosidic bond by Glu478 in Slt70, prolonged binding of GlcNAc in site +1 may prevent the hydrolytic action of a water molecule. The binding of the peptide side-chain at the interface of the catalytic domain and the α-superhelix might be instrumental in preventing an early release of the GlcNAc residue.

A second implication of the Slt70-G(anh)MTri structure is related to the directionality of the Slt70 exo-muramidase activity. In *E. coli* peptidoglycan, all glycan strands start with a GlcNAc residue and end with an anhMurNAc residue (Höltje *et al.*, 1975). According to Beachey *et al.* (1981), Slt70 first binds the GlcNAc end of the glycan strands and then moves into the direction of the anhMurNAc. However, the binding of the 1,6-anhydromuropeptide at sites +1 and +2 and that of the bulgecin A inhibitor at sites −2 and −1 (Thunnissen *et al.*, 1995b) strongly suggest that Slt70 binds the peptidoglycan with the anhMurNAc end in site +2. Since Slt70 has six sugar-binding sites (Thunnissen *et al.*, 1995b), a GlcNAc residue would be bound in site −4, and additional residues connected to this GlcNAc would stick into the solution. A peptidoglycan strand would then bind all six sugar-binding sites in the peptidoglycan-binding groove of Slt70. After completion of the lytic transglycosylase reaction, the strand with the newly formed anhMurNAc moves up from site −1 to site +2, thereby replacing the previously formed 1,6-anhydromuropeptide product, and it is ready to undergo the next cleavage cycle by the enzyme. Movement of the glycan strand further than site +2 is restricted because of the steric obstruction imposed by the superhelical U and L-domains on the peptide crossbridges of the peptidoglycan network.

Future prospects

Although the number of known lytic transglycosylases has increased considerably since the discovery of Slt70, the precise physiological roles of these enzymes have remained elusive. Proposed roles include functions in cell wall growth and cell division (Kohlrausch & Höltje, 1991), in peptidoglycan turnover and recycling (Goodell, 1985), and in making pores into the cell wall to allow transport of DNA or proteins across the peptidoglycan barrier (Dijkstra & Keck, 1996). The availability of high resolution structures of this archetypal member of the lytic transglycosylase family provides now a firm foundation to guide and analyse the results of future studies into the function of lytic transglycosylases. One important aspect in such studies will be to determine whether the lytic transglycosylases exist in specific complexes, and if so, to assess the relevance of such complexes *in vivo* for bacterial cell wall growth and maintenance. The α-superhelix in Slt70 may be required for interactions with other proteins, but unfortunately, at the moment we lack the structural information that could clarify whether indeed protein binding sites are present in Slt70. Insights into the mechanism of peptidoglycan binding and cleavage by Slt70 and the way its lytic activity is regulated, must await crystallographic analysis of the enzyme complexed with various peptidoglycan fragments.

Materials and Methods

Crystallisation, data collection and processing

Purified Slt70 (Betzner & Keck, 1989; Engel *et al.*, 1991) was kindly provided by W. Keck and A. J. Dijkstra, Hoffmann-La Roche, Basel. Crystals of Slt70 were obtained by the hanging drop method using a macroscopic seeding technique (Rozeboom *et al.*, 1990). Briefly, small, single crystals (average dimensions 0.1 mm × 0.05 mm × 0.05 mm), grown from previous crystallisation trials, were selected as seeds. The seeds were carefully washed in a 20% (w/v) saturated ammonium sulphate solution in 0.1 M sodium acetate buffer (pH 5.0). Then, together with 3 µl of the washing solution, single seeds were transferred to siliconised coverslips. Six µl of a protein/buffer solution with 2.5-3 mg/ml Slt70 and 15% ammonium sulphate were added to the droplets. Each drop was equilibrated against 1 ml of a solution containing 20% ammonium sulphate and 0.2 mM dithiothreitol in 0.1 M sodium acetate buffer (pH 5.0). To promote crystal growth while limiting the chance of (secondary) nucleation, the concentration of ammonium sulphate in the reservoir solution was gradually increased to 25% over a period of three weeks. By this method, after six to eight weeks crystals could be obtained with a size (~0.6 mm × 0.2 mm × 0.1 mm) suitable for X-ray diffraction.

Native Slt70 crystallises in space group $P\,2_12_12_1$ with one molecule per asymmetric unit. The crystals contain 63% solvent. At room temperature, the crystals are relatively sensitive to X-ray irradiation and their diffraction power decreases rapidly during the data collection experiment, resulting in an effective resolution of only 2.7 Å resolution (Thunnissen *et al.*, 1994). To improve the diffraction power and to reduce radiation damage during data collection, Slt70 crystals were flash frozen in a stream of cold nitrogen gas. Initially, the crystals were very sensitive towards cryo-protectants like glycerol, ethylene glycol and polyethylene glycol 400. The stability of the crystals could be enhanced by transferring them first from the hanging drop to a stabilisation buffer with an increased ammonium sulphate concentration (50% w/v) and 0.1 M sodium acetate buffer (pH 5.0). Subsequently, the crystals were soaked for two minutes in a cryo-protectant containing 0.1 M sodium acetate buffer (pH 5.0), 50% ammonium sulphate and 26% glycerol. A crystal was flash frozen in a thin fibre loop in a cold nitrogen gas stream (120 K). Under these conditions data could be collected to 1.65 Å resolution using the CCD-detector at the A1 station at CHESS (Cornell High Energy Synchrotron Source) in Ithaca (USA). Data were processed and scaled with DENZO and SCALEPACK

(Otwinowski & Minor, 1997). The unit cell dimensions changed from $a = 80.8$ Å, $b = 88.4$ Å and $c = 132.6$ Å at room temperature to $a = 78.0$ Å, $b = 87.5$ Å and $c = 132.9$ Å at 120 K. The space group did not change.

A soaking experiment with a Slt70 crystal was performed with 1,6-anhydromurotripeptide (G(anh)MTri), which was prepared enzymatically by using immobilized Slt70 fused to staphylococcal protein A (Engel *et al.*, 1992). The crystal was soaked for 31 hours in 50 % (w/v) ammonium sulphate in 0.1 M sodium acetate buffer (pH 5.0), and 5 mM G(anh)MTri. The crystal was flash frozen in a stream of cold nitrogen gas at 120 K, after having been soaked for one minute in a cryo-protectant consisting of the soaking solution with the addition of 26 % glycerol. Using the CCD-detector at the A1 station at CHESS, 1.90 Å and 2.50 Å resolution data sets were collected from a single crystal. The data sets were processed with DENZO and they were scaled and merged with SCALEPACK (Otwinowski & Minor, 1997), which refined to unit cell parameters of $a = 78.3$ Å, $b = 87.5$ Å and $c = 132.9$ Å with $P\,2_12_12_1$ as space group. Data collection statistics are summarized in Table 1.

Refinement of the 1.65 Å resolution model

The 2.7 Å resolution model (Thunnissen *et al.*, 1994) was used as starting structure. After rigid-body refinement at 8.0-3.0 Å resolution, the model was initially refined at 6.0-1.8 Å resolution with a 2σ cut off using X-PLOR version 3.843 (R_{work} of 18.0 % and R_{free} of 22.4 %). The high resolution electron density maps clearly showed that residue 556 was a proline and not a leucine residue, as published in the initial sequence of Slt70 (Engel *et al.*, 1991) and the 2.7 Å resolution structure (Thunnissen *et al.*, 1994). Later, new *E. coli* sequence analyses confirmed our finding (Blattner *et al.*, 1997). Furthermore, in the 2.7 Å resolution structure, residues 374 to 377 had poor electron density. With the new data the main-chain conformation of these residues could be easily fitted into the electron density. Gradually, water molecules were added based on the presence of spherical density above 3σ in $F_o - F_c$ difference Fourier maps and the ability to form at least one hydrogen bond to a neighbouring water molecule or protein hydrogen bond donor or acceptor within 2.4 to 3.5 Å.

In the next refinement cycles, the resolution was extended to include all data between 20.0 and 1.65 Å resolution. This allowed the incorporation of 13 sulphate ions, seven glycerol molecules and one acetate ion in the model. In a later stage of the refinement, alternate conformations were introduced for disordered amino acid side-chains and glycerol molecules. Several solvent molecules showed neighbouring peaks closer than 2.0 Å at the 3.5σ level in $F_o - F_c$ difference maps. If these peaks were at positions that allowed the formation of good hydrogen bonds with neighbouring protein or solvent atoms, they were introduced as alternate positions for solvent molecules. The occupancies of the alternate positions and conformations were refined and normalised to a total occupancy of 1.0 in X-PLOR. In the final refinement cycles, data between 20.0 and 1.65 Å resolution without any sigma cut off were used, whereby a bulk solvent correction, an overall anisotropic *B*-factor scaling, resolution dependent weighting and $(1/\sigma^2)$ weighting were applied. The final refinement statistics are summarised in Table 1.

Refinement of the Slt70-1,6-anhydromuropeptide model

Refinement of the Slt70-1,6-anhydromuropeptide complex was started from the coordinates of the native Slt70 model refined at 1.65 Å resolution to an R_{work} of 16.8 % and R_{free} of 19.1 %. All refinement steps were carried out using the program X-PLOR version 3.843. To establish a test set for cross-validation during the refinement, 50 % of the reflections present in the native 1.65 Å test set were randomly selected (in total 5 % of the 1.90 Å data). First, a rigid-body refinement of the native Slt70 model was performed at 8-3.5 Å resolution to optimise the orientation and position of the Slt70 molecule in the asymmetric unit. Then the model was further refined using several rounds of conjugate-gradient energy minimisation and overall *B*-factor refinement with $|F| > 0$, a bulk solvent correction to the low resolution data and an overall anisotropic *B*-factor scaling to F_{calc}. Resolution-dependent two-line weighting and sigma weighting $(1/\sigma^2)$ schemes were applied to the data for the refinement of the Slt70-G(anh)MTri model. Solvent molecules and alternative side-chain conformations derived from the native Slt70 structure were removed from the model, if they had no or weak electron density. Additional solvent molecules were added to the protein model based on the presence of spherical density in σ_A-weighted $F_o - F_c$ and $2F_o - F_c$ maps at contour levels of 3σ and 1σ, respectively, and the ability to form at least one hydrogen bond to a neighbouring water molecule or protein residue with a distance between 2.4 and 3.5 Å. At this stage the electron density corresponding to the muropeptide was clearly visible in $2F_o - F_c$ and $F_o - F_c$ Fourier maps, and a model of the compound was fitted into the electron density using the program O (Jones *et al.*, 1991). The force constants and parameters used for the GlcNAc sugar were those described by Weis *et al.* (1990) as implemented in the X-PLOR geometry files. Bond angles and distances for the 1,6-anhydromuramic acid residue of the G(anh)MTri compound were based on the X-ray structures of 1,6-anhydro sugars in the Cambridge Structural Database. Dihedral angles defining the conformation of the sugar rings were not explicitly restrained. A grouped *B*-factor refinement was applied to the new solvent and sugar compounds. Because of the low completeness of the data, an individual *B*-factor refinement did not improve the R_{free} and was therefore not applied in the refinement cycles. The last refinement cycle was repeated for all reflections including the test set. Table 1 summarises the data collection and the final statistics on the Slt70-G(anh)MTri structure.

Structure analysis

The stereochemical quality of the protein model was analysed with the PROCHECK (Laskowski *et al.*, 1993), PROMOTIF (Hutchinson & Thornton, 1996) and WHATCHECK (Hooft *et al.*, 1996) software. Additional structure analysis was performed using various programs from the Groningen BIOMOL package and CCP4 (CCP4, 1994) software package. Interhelical distances and angles were calculated using PROMOTIF. Interatomic distances and hydrogen bond interactions were calculated with CONTACTS (CCP4 package), accessible surface areas with ASC (Eisenhaber & Argos, 1993), and real space correlation coefficients with OVERLAPMAP (CCP4, 1994).

Accession numbers

The Slt70 coordinates and X-ray amplitudes have been deposited with the Protein Data Bank (entries 1QSA for the native Slt70 structure, and 1QTE for the Slt70-G(anh)MTri complex structure, respectively).

Acknowledgements

We thank M. Szebenyi and D. Thiel for their help during data collection at the A1 station in CHESS, and A.J. Dijkstra and W. Keck (F. Hoffmann-La Roche Ltd., Basel) for the supply of protein and 1,6-anhydromuropeptide, and stimulating discussions. E.J.v.A. and A.M.W.H.T. contributed equally to the work reported in this paper. This work was supported by the Netherlands Foundation for Chemical Research (SON) with financial aid from the Netherlands Organization for Scientific Research (NWO).

References

Aleshin, A., Golubev, A., Firsov, L. M. & Honzatko, R. B. (1992). Crystal structure of glucoamylase from *Aspergillus awamori* var. X100 to 2.2-Å resolution. *J. Bacteriol.* **267**, 19291-19298.

Altschul, S. F., Madden, T. L., Schiffer, A. A., Zhang, J., Zhang, Z., Miller, W. & Lipman, D. J. (1997). Gapped BLAST and PHI-BLAST: a new generation of protein database search programs. *Nucl. Acids Res.* **25**, 3389-3402.

Anderson, T. A., Levitt, D. G. & Banaszak, L. J. (1998). The structural basis of lipid interactions in lipovitellin, a soluble lipoprotein. *Structure,* **6**, 895-909.

Banic, Z., Kojic-Prodic, B., Kroon-Batenburg, L. & Keglevic, D. (1994). Conformational analysis and computer modelling of muramic acid δ-lactam structures. *Carbohydr. Res.* **259**, 159-174.

Barton, G. J. (1993). ALSCRIPT: a tool to format multiple sequence alignments. *Protein Eng.* **6**, 37-40.

Baumann, U., Wu, S., Flaherty, K. M. & McKay, D. B. (1993). Three-dimensional structure of the alkaline protease of *Pseudomonas aeruginosa*: a two domain protein with a calcium binding parallel β-roll motif. *EMBO J.* **12**, 3357-3364.

Beachey, E. H., Keck, W., de-Pedro, M. A. & Schwarz, U. (1981). Exoenzymatic activity of transglycosylase isolated from *Escherichia coli*. *Eur. J. Biochem.* **116**, 355-358.

Betzner, A. S. & Keck, W. (1989). Molecular cloning, overexpression and mapping of the *slt* gene encoding the soluble lytic transglycosylase of *Escherichia coli*. *Mol. Gen. Genet.* **219**, 489-491.

Blattner, F. R., Plunkett, G., III, Bloch, C. A., Perna, N. T., Burland, V., Riley, M., Collado, Vides J., Glasner, J. D., Rode, C. K., Mayhew, G. F., Gregor, J., Davis, N. W., Kirkpatrick, H. A., Goeden, M. A., Rose, D. J., Mau, B. & Shao, Y. (1997). The complete genome sequence of *Escherichia coli* K-12. *Science,* **277**, 1453-1474.

CCP4 (1994). Collaborative Computational Project Number 4 - The CCP4 suite: programs for protein crystallography. *Acta Crystallog. sect. D,* **50**, 760-763.

Chothia, C. (1984). Principles that determine the structure of proteins. *Annu. Rev. Biochem.* **53**, 537-572.

Chothia, C., Levitt, M. & Richardson, D. (1981). Helix to helix packing in proteins. *J. Mol. Biol.* **145**, 215-250.

Cingolani, G., Petosa, C., Weis, K. & Müller, C. W. (1999). Structure of importin-β bound to the IBB domain of importin-α. *Nature,* **399**, 221-229.

Cookson, B. T., Cho, H.-L., Herwaldt, L. A. & Goldman, W. E. (1989). Biological activities and chemical composition of purified tracheal cytotoxin of *Bordetella pertussis*. *Infect. Immun.* **57**, 2223-2229.

Davies, G. & Henrissat, B. (1995). Structures and mechanisms of glycosyl hydrolases. *Structure,* **3**, 853-859.

Dijkstra, A. J. (1997). The soluble lytic transglycosylase family of Escherichia coli. In vitro activity versus in vivo function. PhD thesis, University of Groningen.

Dijkstra, A. J. & Keck, W. (1996). Peptidoglycan as a barrier to transenvelope transport. *J. Bacteriol.* **178**, 5555-5562.

Dijkstra, A. J., Hermann, F. & Keck, W. (1995). Cloning and controlled overexpression of the gene encoding the 35 kDa soluble lytic transglycosylase from *Escherichia coli*. *FEBS Letters,* **366**, 115-118.

Dokter, W. H., Dijkstra, A. J., Koopmans, S. B., Stulp, B. K., Keck, W., Halie, M. R. & Vellenga, E. (1994). G(Anh)MTetra, a natural bacterial cell wall breakdown product, induces interleukin-1 beta and interleukin-6 expression in human monocytes. A study of the molecular mechanisms involved in inflammatory cytokine expression. *J. Biol. Chem.* **269**, 4201-4206.

Ehlert, K., Höltje, J.-V. & Templin, M. F. (1995). Cloning and expression of a murein hydrolase lipoprotein from *Escherichia coli*. *Mol. Microbiol.* **16**, 761-768.

Eisenhaber, F. & Argos, P. (1993). Improved strategy in analytic surface calculation for molecular systems: handling of singularities and computational efficiency. *J. Comp. Chem.* **14**, 1272-1280.

Engel, H., Kazemier, B. & Keck, W. (1991). Murein-metabolizing enzymes from *Escherichia coli*: sequence analysis and controlled overexpression of the *slt* gene, which encodes the soluble lytic transglycosylase. *J. Bacteriol.* **173**, 6773-6782.

Engel, H., van Leeuwen, A., Dijkstra, A. & Keck, W. (1992). Enzymatic preparation of 1,6-anhydro-muropeptides by immobilized murein hydrolases from *Escherichia coli* fused to staphylococcal protein A. *Appl. Microbiol. Biotechnol.* **37**, 772-783.

Engh, R. A. & Huber, R. (1991). Accurate bond and angle parameters for X-ray protein structure refinement. *Acta Crystallog. sect. A,* **47**, 392-400.

Gaykema, W. P. J., Hol, W. G. J., Vereijken, M., Soeter, N. M., Bak, H. J. & Beintema, J. J. (1984). 3.2 Å structure of the copper-containing oxygen-carrying protein *Panulirus interruptus* haemocyanin. *Nature,* **309**, 23-29.

Goodell, E. W. (1985). Recycling of murein in *Escherichia coli*. *J. Bacteriol.* **163**, 305-310.

Groves, M. R., Hanlon, N., Turowski, P., Hemmings, B. A. & Barford, D. (1999). The structure of the protein phosphatase 2A PR65/A subunit reveals the conformation of its 15 tandemly repeated HEAT motifs. *Cell,* **96**, 99-110.

Hamada, K., Bethge, P. H. & Mathews, F. S. (1995). Refined structure of cytochrome b562 from *Escherichia coli* at 1.4 Å resolution. *J. Mol. Biol.* **247**, 947-962.

Hol, W. G. J. (1985). The role of the α-helix dipole in protein function and structure. *Prog. Biophys. Mol. Biol.* **45**, 149-195.

Höltje, J.-V. (1996). Molecular interplay of murein synthases and murein hydrolases in *Escherichia coli*. *Microb. Drug Resist.* **2**, 99-103.

Höltje, J.-V. (1998). Growth of the stress-bearing and shape-maintaining murein sacculus of *Escherichia coli*. *Microbiol. Mol. Biol. Rev.* **62**, 181-203.

Höltje, J.-V. & Schwarz, U. (1985). Biosynthesis and growth of the murein sacculus. In *Molecular Cytology of* Escherichia coli, pp. 77-119, Academic Press, London.

Höltje, J.-V., Mirelman, D., Sharon, N. & Schwarz, U. (1975). Novel type of murein transglycosylase in *Escherichia coli*. *J. Bacteriol.* **124**, 1067-1076.

Hooft, R. W. W., Vriend, G., Sander, C. & Abola, E. E. (1996). Errors in protein structures. *Nature,* **381**, 272.

Huber, A. H., Nelson, W. J. & Weis, W. I. (1997). Three-dimensional structure of the armadillo repeat region of β-catenin. *Cell,* **90**, 871-882.

Huber, R., Römisch, J. & Paques, E.-P. (1990). The crystal and molecular structure of human annexin V, an anticoagulant protein that binds to calcium and membranes. *EMBO J.* **9**, 3867-3874.

Hutchinson, E. G. & Thornton, T. M. (1996). PROMOTIF - a program to identify and analyze structural motifs in proteins. *Protein Sci.* **5**, 212-220.

Janin, J., Miller, S. & Chothia, C. (1988). Surface, subunit interface and interior of oligomeric proteins. *J. Mol. Biol.* **204**, 155-164.

Johannsen, L. (1993). Biological properties of bacterial peptidoglycan. *Acta Pathol. Microbiol. Immunol. Scand.* **101**, 337-344.

Jones, T. A., Zou, J.-Y., Cowan, S. W. & Kjeldgaard, M. (1991). Improved methods for building protein models in electron density maps and the location of the errors in these models. *Acta Crystallog. sect. A,* **47**, 110-119.

Juy, M., Amit, A. G., Alzari, P. M., Poljak, R. J., Claeyssens, M., Béguin, P. & Aubert, J.-P. (1992). Three-dimensional structure of a thermostable bacterial cellulase. *Nature,* **357**, 89-91.

Kobe, B. (1999). Autoinhibition by an internal nuclear localization signal revealed by the crystal structure of mammalian importin α. *Nature Struc. Biol.* **6**, 388-397.

Kobe, B. & Deisenhofer, J. (1993). Crystal structure of porcine ribonuclease inhibitor, a protein with leucine-rich repeats. *Nature,* **366**, 751-756.

Kobe, B., Gleichmann, T., Horne, J., Jennings, I. G., Scotney, P. D. & Tey, T. (1999). Turn up the HEAT. *Structure,* **7**, R91-R97.

Kohlrausch, U. & Höltje, J.-V. (1991). Analysis of murein and murein precursors during antibiotic-induced lysis of *Escherichia coli*. *J. Bacteriol.* **173**, 3425-3431.

Kraft, A. R., Templin, M. F. & Höltje, J.-V. (1998). Membrane-bound lytic endoglycosylase in *Escherichia coli*. *J. Bacteriol.* **180**, 3441-3447.

Kuroki, R., Weaver, L. H. & Matthews, B. W. (1993). A covalent enzyme-substrate intermediate with saccharide distortion in a mutant T4 lysozyme. *Science,* **262**, 2030-2033.

Laskowski, R. A., MacArthur, M. W., Moss, D. S. & Thornton, J. M. (1993). PROCHECK: a program to check the stereochemical quality of protein structures. *J. Appl. Crystallog.* **26**, 283-291.

Lawson, C. L., van Montfort, R., Strokopytov, B., Rozeboom, H. J., Kalk, K. H., de Vries, G. E., Penninga, D., Dijkhuizen, L. & Dijkstra, B. W. (1994). Nucleotide sequence and X-ray structure of cyclodextrin glycosyltransferase from *Bacillus circulans* strain 251 in a maltose-dependent crystal form. *J. Mol. Biol.* **236**, 590-600.

Lommatzsch, J., Templin, M. F., Kraft, A. R., Vollmer, W. & Höltje, J.-V. (1997). Outer membrane localization of murein hydrolases: MltA, a third lipoprotein lytic transglycosylase in *Escherichia coli*. *J. Bacteriol.* **179**, 5465-5470.

Martin, S. A., Karnovsky, M. L., Krueger, J. M., Pappenheimer, J. R. & Biemann, K. (1984). Peptidoglycan as promoters of slow-wave sleep: 1. Structure of the sleep-promoting factor isolated from human urine. *J. Biol. Chem.* **259**, 12652-12658.

Meinke, A., Gilkes, N. R., Kilburn, D. G., Miller, R. C. J. & Warren, R. A. J. (1991). Multiple domains in Endoglucanase B (CenB) from *Cellulomonas fimi*: functions and relatedness to domains in other polypeptides. *J. Bacteriol.* **173**, 7126-7135.

Melly, M. A., McGee, Z. A. & Rosenthal, R. S. (1984). Ability of monomeric peptidoglycan fragments from *Neisseria gonorrhoeae* to damage human fallopian-tube mucosa. *J. Infect. Dis.* **149**, 378-386.

Morris, A. L., MacArthur, M. W., Hutchinson, E. G. & Thornton, J. M. (1992). Stereochemical quality of protein structure coordinates. *Proteins: Struct. Funct. Genet.* **12**, 345-364.

Otwinowski, Z. & Minor, W. (1997). Processing of X-ray diffraction data collection in oscillation mode. *Methods Enzymol.* **276**, 307-326.

Paliakasis, C. D. & Kokkinidis, ?. (1992). Relationships between sequence and structure for the four-α-helix bundle tertiary motif in proteins. *Protein Eng.* **5**, 739-748.

Park, H.-W., Boduluri, S. R., Moomaw, J. F., Casey, P. J. & Beese, L. S. (1997). Crystal structure of protein farnesyltransferase at 2.25 Å resolution. *Science,* **275**, 1800-1804.

Presnell, S. R. & Cohen, F. E. (1989). Topological distribution of four-α-helix bundles. *Proc. Natl Acad. Sci. USA,* **86**, 6592-6595.

Read, R. J. (1986). Improved Fourier coefficients for maps using phases from partial structures with errors. *Acta Crystallog. sect. A,* **42**, 140-149.

Romeis, T., Kohlraus, U., Burgdorf, K. & Höltje, J.-V. (1991). Murein chemistry of cell division in *Escherichia coli*. *Res. Microbiol.* **142**, 325-332.

Romeis, T., Vollmer, W. & Höltje, J.-V. (1993). Characterization of three different lytic transglycosylases in *Escherichia coli*. *FEMS Microbiol. Letters,* **111**, 141-146.

Rozeboom, H. J., Dijkstra, B. W., Engel, H. & Keck, W. (1990). Crystallization of the soluble lytic transglycosylase from *Escherichia coli* K12. *J. Mol. Biol.* **212**, 557-559.

Schwarz, U., Asmus, A. & Frank, H. (1969). Autolytic enzymes and cell division of *Escherichia coli*. *J. Mol. Biol.* **41**, 419-429.

Sheldrick, G. M. & Schneider, T. R. (1997). SHELXL: high resolution refinement. *Methods Enzymol.* **277**, 319-343.

Shockman, G. D. & Höltje, J.-V. (1994). *Microbial peptidoglycan (murein) hydrolases. Bacterial cell wall* (Ghuysen, J.-M. & Hakenbeck, R., eds), Elsevier Science B. V., Amsterdam.

Templin, M. F., Edwards, D. H. & Höltje, J.-V. (1992). A murein hydrolase is the specific target of bulgecin in *Escherichia coli*. *J. Biol. Chem.* **267**, 20039-20043.

Thompson, J. D., Higgins, D. G. & Gibson, T. J. (1994). CLUSTAL W: improving the sensitivity of progressive multiple sequence alignment through sequence

weighting, positions-specific gap penalties and weight matrix choice. *Nucl. Acids Res.* **22**, 4673-4680.

Thunnissen, A.-M. W. H., Dijkstra, A. J., Kalk, K. H., Rozeboom, H. J., Engel, H., Keck, W. & Dijkstra, B. W. (1994). Doughnut-shaped structure of a bacterial muramidase revealed by X-ray crystallography. *Nature,* **367**, 750-753.

Thunnissen, A.-M. W. H., Isaacs, N. W. & Dijkstra, B. W. (1995a). The catalytic domain of a bacterial lytic transglycosylase defines a novel class of lysozymes. *Proteins: Struct. Funct. Genet.* **22**, 245-258.

Thunnissen, A.-M. W. H., Rozeboom, H. J., Kalk, K. H. & Dijkstra, B. W. (1995b). Structure of the 70-kDa soluble lytic transglycosylase complexed with bulgecin A. Implications for the enzymatic mechanism. *Biochemistry*, **34**, 12729-12737.

Ursinus, A. & Höltje, J.-V. (1994). Purification and properties of a membrane-bound lytic transglycosylase from *Escherichia coli*. *J. Bacteriol.* **176**, 338-343.

von Rechenberg, M., Ursinus, A. & Höltje, J.-V. (1996). Affinity chromatography as a means to study multienzyme complexes involved in murein synthesis. *Microb. Drug Resist.* **2**, 155-157.

Walderich, B. & Höltje, J.-V. (1991). Subcellular distribution of the soluble lytic transglycosylase in *Escherichia coli*. *J. Bacteriol.* **173**, 5668-5676.

Wallace, A. C., Laskowski, R. A. & Thornton, J. M. (1995). LIGPLOT: a program to generate schematic diagrams of protein-ligand interactions. *Protein Engin.* **8**, 127-134.

Waxman, D. J. & Strominger, J. L. (1983). Penicillin-binding proteins and the mechanism of action of β-lactam antibiotics. *Annu. Rev. Biochem.* **52**, 825-869.

Weber, P. C. & Salemme, F. R. (1980). Structural and functional diversity in 4-α-helical proteins. *Nature,* **287**, 82-84.

Weidel, W. & Pelzer, H. (1964). Bag-shaped macromolecules - a new outlook on bacterial cell walls. *Advan. Enzymol.* **26**, 193-232.

Weis, W. I., Brünger, A. T., Skehel, J. J. & Wiley, D. C. (1990). Refinement of the influenza virus hemagglutinin by simulated annealing. *J. Mol. Biol.* **212**, 737-761.

White, A. & Rose, D. R. (1997). Mechanism of catalysis by β-glycosyl hydrolases. *Curr. Opin. Struct. Biol.* **7**, 645-651.

Yoder, M. D., Lietzke, S. E. & Jurnak, F. (1993). Unusual structural features in the parallel β-helix in pectate lyases. *Structure,* **1**, 241-251.

Edited by K. Nagai

(Received 12 May 1999; received in revised form 5 July 1999; accepted 7 July 1999)